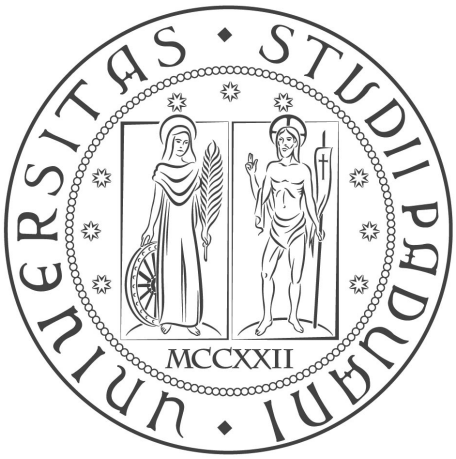

Università degli Studi di Padova

Dipartimento di Ingegneria Industriale

Tesi di Laurea Magistrale in Ingegneria Aerospaziale

Anno accademico 2014-2015

Mass transfer in media of variable porosity

Relatore: *Prof. F. Picano*
Correlatore: *Prof. L. Brandt*
Correlatore: *Ing. I. Lashgari*
Controrelatore: *Prof. A. Marion*

Laureando: *Enrico Fidelfatti*
Matricola: *1084085*

Il meglio è ancora tutto da fare

Sfruttando a fondo ogni opportunità

Senza subire il destino

Con tanta forza di volontà

Abstract

Transport of scalar quantities in porous media is crucial in several different fields from geophysical problems to industrial applications. E.g. in the context of energy accumulation devices for the civil and aerospace sectors, Redox-flow Battery and Fuel Cells are ideal candidates and use porous media as the electrodes where the fluids flow and react. The peak performance and the efficiency of these devices is limited by the slow diffusion process acting in the porous media. Given the constrains on weight and sizes, especially in the aerospace industry, an enhancement of the mass transfer and mixing is crucial. The aim of this thesis project is to study how a modulation of the porosity of the media affects the mass transfer. The effectiveness of mixing is evaluated by analyzing a flow in a porous channel where the distribution of the porosity is varied in different ways. To this purpose Direct Numerical Simulations have been performed using the open-source parallel code NEK5000. This tool developed at Argonne National Laboratories uses spectral element method to solve numerically the equations for fluid and scalar evolutions. The code has been expanded during this thesis project to allow the solutions of the Volume Average Navier-Stokes equations for flows in a porous media with different local porosity. The simulations have been performed fixing all the controlling parameters, such as the bulk porosity (0.7), while the modulation of the local porosity has been changed using harmonic functions with different wave numbers. Different cases pertaining to steady- and transient- state problems have been analyzed.

We found that using a non-uniform porosity it is possible to increase the mass flux and the mixing up to 40%. Generally we observe that porosity modulation at lower wavenumbers is the most effective. We also propose a criterion to determine the optimal modulation along the three directions based on dimensional consideration on the typical time diffusive and advective time scales.

Sommario

Il trasporto di quantià scalari attraverso mezzi porosi è cruciale in molte applicazioni, dal campo aerospaziale a problemi geofisici. Ad esempio, nei dispositivi per accumulo di energia utilizzati sia nel campo civile che in quello aerospaziale, le batterie a combustibile e quelle a flusso risultano candidate ideali. Queste tipologie di batterie utilizzano mezzi porosi come elettrodi, i quali sono attraversati dal fluido che reagisce al loro interno. La massima resa ed efficienza di questi dispositivi è limitata dal lento processo di diffusione che avviene all'interno del mezzo poroso. Considerando la presenza di limiti nel loro peso e dimensioni, soprattutto nel campo aerospaziale, l'incrememento del trasporto di massa e del mixing è di fondamentale importanza. L'obiettivo di questa tesi è lo studio di come il trasporto di massa è influenzato dalla modulazione della porosità nel mezzo. L'efficacia del mixing è valutato analizzando il flusso in un canale poroso in cui la modulazione della distribuzione di porosità è variata in diversi modi. A questo scopo sono state eseguite simulazione numeriche dirette (DNS) utilizzando NEK5000, un codice di calcolo parallelo open-source. Questo software, sviluppato da Argonne National Laboratories, applica il metodo degli elementi spettrali per risolvere numericamente le equazioni dei fluidi e dello scalare. Durante lo svolgimento della tesi, questo codice è stato espanso per permettere la risoluzione delle Volume Average Navier Stokes equations, le quali caratterizzano il moto dei fluidi nei mezzi porosi con valori locali di porosità differenti. Nelle simulazioni sono stati fissati e man-

tenuti costanti i parametri di controllo, come ad esempio il valore della porosità media (0.7), mentre le modulazioni locali della porosità sono state modificate usando funzioni armoniche con differenti lunghezze d'onda. Sono stati analizzati sia casi in condizione di stazionarietà e sia nel transitorio. E' stato riscontrato che utilizzando una porosità non uniforme è possibile aumentare il flusso di massa, e quindi il mixing, attorno a valori del 40% superiori. Generalemente si osserva che modulando la porosità con basse lunghezze d'onda si ottiene una efficacia maggiore. E' inoltre proposto un criterio per l'ottimizzazione della modulazione della porosità nelle tre direzioni basato in un analisi dimensionale dei tempi caratteristici di diffusione e convezione.

Contents

Chapter 1

Introduction

Flows inside porous media are largely encountered in industrial applications and environmental systems, such as the electrodes of fuel cells, ground flows and oil extraction process.

Even in aerospace industries there are many different applications involving porous media. E.g., flows inside a porous media are studied to developed a new class of flow batteries (Redox Flow Battery and Fuel Cell) for aerospace energy storage applications. For example, NASA is currently seeking high-specific-energy and long-cycle-life rechargeable batteries in the 10-to-100-kW power range to support future human exploration missions, such as planetary habitats, human rovers, etc. In these applications porous carbon electrodes are used and they shown better kinetics than other materials used, yielding higher discharge currents [Bugga *et al.*(2013)Bugga, West, Kindler & Smart]. The bottleneck in these problems is often constituted by the species transport in the porous media which acts as reactive electrode. In these problems the flow is always laminar and the typically small diffusion coefficients induce a relatively small effective transport. The usual enhancement of the mixing induced by turbulence is absent in these applications making the advective transport not effective.

Hence the aim of this project is to study if a non uniform porosity of the medium can be effective in enhancing the mixing inducing secondary flow motions. A fundamental numerical approach is adopted to address the problem. In particular the open source code NEK5000 developed at Argonne National Laboratories has been adopted and modified to deal with flows and mass transport in porous media. The channel flow configuration has been selected using different porous media. The porous media are characterized by different spatial distribution of the porosity prescribed by corresponding harmonic functions. The typical parameters of the simulations have been selected to lie in the range of fuel cells and Redox Flow Battery applications. Two main classes of simulations have been performed. In the former a jump in the scalar concentration field is imposed on the upper and lower surfaces, which mimics a process where the transport occur between two (reactive) walls with a cross flow. In the second, we focused on the time needed to move from a inhomogeneous mass concentration across the channel to a homogeneous distribution. In both cases, when the fluid flows through a medium with a non-uniform porosity distribution, the mean flow is modified and secondary cross-stream motions take place affecting the mass transfer between the walls.

The main difference between the two methods is that the former pertains to steady applications, while the second one is more appropriate to reproduce transient phenomena.

The results reported in this work demonstrate that a non-uniform porosity is able to induce motions in the transfer direction (across the surfaces with different mass concentrations) enhancing the mixing and the overall mass transfer. The porosity distribution that maximizes the mass transfer is not the same for the two classes of problems. An explanation of this difference is proposed in this thesis. Moreover for the first class of problems (steady-state) a criterion based on the ratio between the typical diffusion and advection time scales is proposed to interpret the data and

design the optimal porosity distribution.

The thesis is divided into six chapters. Single-phase flows are introduced in Chapter 2 together with the laws governing flow dynamics. The third chapter focuses on porous media description and the equations governing the flow through a porous media are obtained. The fourth chapter presents the methodology used in this project. In particular, the computational fluid dynamics method is briefly presented and the new implementation on the code used (NEK5000) explained. The following two chapters show the results obtained in the two different configuration classes mentioned before. In the last chapter the conclusions and the perspectives obtained by the present work are outlined.

Chapter 2

Single-Phase Flows

In this first chapter the single-phase flows are introduced. Firstly, the definition and main characteristics of fluids are presented. In the second part, the equations that describe fluid flow dynamics are shown together with the passive scalar transport equation. The last section focuses on the theory of non-dimensional analysis, which is really important in this project to obtain the dimension-less parameters to describe the fluid phenomena.

2.1 Fluids

In physics, a fluid is defined a substance that continually deforms (flows) under an applied shear stress and cannot resist any shear force applied to it. The distinction between solids and fluids is due to viscosity, a solid has a preferred shape while a fluid takes the shape of its container. More precisely, we can define a fluid as a substance that deforms continuously under the action of a shear force, however small. It is important to specify "however small" because solids also deform continuously if the shear stress exceeds a certain limiting value, corresponding to the "yield point" of the solid (plastic behavior). Even so, if the shear stress is less than

the "yield point" when removed the solid returns to his originally shape (elastic behavior). Instead, fluid never returns to the preferred shape when the shear stress is removed. Another important difference is that a solid can support tension and compression, the fluid only compression.

Fluids are a subset of the phases of matter and include liquids, gases and plasmas. Gas tend to occupy all the volume of the container, so their density changes significantly. Instead fluids do not change their density for different types of container, so their density can usually be considered constant ; plasma are ionized gas , consisting of a set of electrons and ions and globally neutral [Kundu P.K.(2004)].

A fluid is composed of a large number of molecules in constant motion and undergoing collisions which each other. Matter is therefore discontinuous or discrete at microscopic scales. In principle, it is possible to study the mechanics of a fluid by studying the motion of the molecules themselves, but usually it is interesting to know only the gross behavior of the fluid, i.e the average manifestation of the molecular motion. It is possible to ignore the discrete molecular structure of matter and replace it by a continuous distribution. The Knudesen Number defined as the ratio between the molecular mean free path and the smallest geometric length scale in a flow tell us when it is correct to use the continuum approximation. If this ratio is much smaller than 1, the continuum hypothesis is correct.

There are two ways of describing the motion of fluid. In the Lagrangian description, one essentially follows the history of individual fluid particles and consequently the two independent variables are time and a label for fluid particles (which by definition moves with the local fluid velocity). In the Eulerian description, instead, one studies the behavior at a fixed spatial point, so that the independent variables are the position in an inertial frame and time.

The link between these two approaches is provided by the material derivative. Let **F** be any field variable with Eulerian specification **F**(**x**,t), in the presence if a flow

field **u**: the total rate of change of **F** (the derivative is taken following a fluid element) is written as:

$$\frac{D\mathbf{F}}{Dt} = \frac{\partial \mathbf{F}}{\partial t} + \mathbf{u}_i \frac{\partial \mathbf{F}}{\partial x_i} \tag{2.1}$$

It is made of two parts: $\frac{\partial \mathbf{F}}{dt}$ is the local rate of change of **F** at a given point (eulerian derivative) and $\mathbf{u}_i \frac{\partial \mathbf{F}}{dx_i}$ is the change in **F** as a result of advection of the particle (due to the underlying flow **u**) from one location to another where the value of **F** is different (convection or advection derivative) [Kundu P.K.(2004), Pope(2000)].

Following these considerations, we use the fundamental physical principles

- mass conservation
- Newton's second law of motion
- Energy conservation

to obtain the equation of fluid dynamics. These equations are complicated to treat and do not have an analytical solution for most cases. For this reason, it is often necessary to use numerical methods to solve them. Computational fluid dynamics, usually abbreviated as CFD, is a branch of fluid mechanics that uses numerical analysis and algorithms to solve and analyze problems that involve fluid flows. These method showed his potential only during the last years thanks to the increase of computer calculation power. [Jhon D. Anderson(2001)]

2.2 Fluid Dynamics

Fluid dynamics is the branch of fluid mechanics focused on the study of fluid flows. The foundational axioms of fluid dynamics are the conservation laws, specifically, conservation of mass, conservation of linear momentum (also known as Newton's Second Law of Motion), and conservation of energy (also known as First Law of

Thermodynamics). In addition to the above, fluids are assumed to obey the continuum assumption as already discussed in the previous section.

In addition to the mass, momentum, and energy conservation equations, a thermodynamical equation of state giving the pressure as a function of other thermodynamic variables for the fluid is required to completely specify the problem. An example of this would be the perfect gas equation of state:

$$p = \frac{\rho R_u T}{M} \tag{2.2}$$

where p is pressure, ρ is density, R_u is the gas constant, M is molar mass and T is temperature.

These equations are used to solve fluid dynamics problems, and may be written in integral or differential form. Mathematical formulations of these conservation laws may be interpreted by considering the concept of a control volume. A control volume is a specified volume in space through which fluid can flow in and out. Integral formulations of the conservation laws consider the change in mass, momentum, or energy within the control volume. Differential formulations of the conservation laws apply Stokes' theorem to yield an expression which may be interpreted as the integral form of the law applied to an infinitesimal volume at a point within the flow.

- Mass continuity (conservation of mass): The rate of change of fluid mass inside a control volume must be equal to the net rate of fluid flow into the volume. The integral form of the continuity equation:

$$\underbrace{\frac{\partial}{\partial t}\iiint_V \rho dV}_{rate of mass change} = \underbrace{-\oiint_S \rho \mathbf{u} \cdot d\mathbf{S}}_{mass flow from boundaries} \tag{2.3}$$

  where ρ is the fluid density, $\mathbf{u}$ is the flow velocity vector and t is time. The

differential form of the continuity equation is, by the divergence theorem:

$$\frac{\partial \rho}{\partial t} + \nabla \cdot (\rho \mathbf{u}) = 0 \tag{2.4}$$

- Conservation of momentum: This equation applies Newton's second law of motion to the control volume, requiring that any change in momentum within a control volume be due to the net momentum flow into the volume and the action of external forces on the fluid within the volume.

$$\frac{\partial}{\partial t} \iiint_V \rho \mathbf{u} dV = - \oiint_S (\rho \mathbf{u} \cdot dS)\mathbf{u} - \oiint_S p d\mathbf{S} + \iiint_V \rho \mathbf{f}_{body} dV + \mathbf{F}_{surf} \tag{2.5}$$

where p is the pressure, $\mathbf{f}_{body}$ is the body force per unit mass and $\mathbf{F}_{surf}$ are the surface forces due to stresses on the control volume surface. The differential form of the momentum conservation equation is as follows.

$$\rho \frac{\partial \mathbf{u}}{\partial t} + \rho \mathbf{u} \cdot \nabla \mathbf{u} = -\nabla p + \nabla \cdot \boldsymbol{\tau} + \rho \mathbf{f}_{body} \tag{2.6}$$

and $\boldsymbol{\tau}$ is the tensor of viscous stresses.

- Conservation of energy: although energy can be converted from one form to another, the total energy in a given closed system is conserved. The integral form is

$$\oiiint_V \dot{q} \rho dV + \dot{Q} - \oiint_S p \mathbf{u} \cdot \mathbf{dS} + \oiiint_V \rho (\mathbf{f}_b ody \cdot \mathbf{u} dV + \dot{W}_{viscous} = \frac{\partial}{\partial t} \oiiint_V \rho h dV + \oiint_S \rho h \mathbf{u} \cdot \mathbf{dS} \tag{2.7}$$

where $\dot{q}$ is the volumetric rate of heat addition per unit mass, $\dot{Q}_{viscous}$ is the rate of heat addition to the control volume due to viscous effects, $\dot{W}_{viscous}$ is the shear stress work on the fluid and h is the enthalpy. As usual, it is

presented also in the differential form:

$$\rho\frac{\partial h}{\partial t} + \nabla\cdot(\rho h\mathbf{u} = \rho\dot{q} - \nabla\cdot(p\mathbf{u}) \\ + \rho(\mathbf{f}_{body}\cdot\mathbf{u}) + \dot{Q}_{viscous} + \dot{W}_{viscous} \tag{2.8}$$

Note that, if the flow is steady, meaning that its properties do not change over time, all time-dependent terms in the above equations disappear.

2.2.1 Navier-Stokes equations

From the eq. 2.6 it is possible to obtain the well-know Navier-Stokes equations for viscous flows. These balance equations arise from applying Newton's second law to fluid motion, together with the assumption that the stress in the fluid is the sum of a viscous term (proportional to the gradient of velocity) and an isotropic pressure term.

For most of the usual fluids, such as air or water, the tensor of viscous stresses is given by the Newtonian law:

$$\boldsymbol{\tau} = \frac{2}{3}\mu\mathbf{I}\nabla\cdot\mathbf{u} + 2\mu\mathbf{D} \tag{2.9}$$

where μ is the dynamic viscosity and $\mathbf{D}$ is the tensor of strain rate:

$$D_{i,j} = \frac{1}{2}\left(\frac{\partial u_i}{\partial x_j} + \frac{\partial u_j}{\partial x_i}\right) \tag{2.10}$$

If the fluid has a tensor of viscous stresses linearly dependent to the tensor of strain rate, Eq. 2.9, it is called Newtonian fluid, otherwise it is said to be non-Newtonian. If the tensor of viscous stresses $\boldsymbol{\tau}$ is instead null, the flow is said to be non-viscous.

The flows studied in this work are incompressible: a flow is compressible if

a change in pressure or temperature results in a change of the density; if this does not happen, or if the change of the density is negligible, the flow is incompressible. The equations of motion for a Newtonian incompressible fluid is obtained by substituting eq. 2.9 into eq. 2.6 to obtain the incompressible Navier-Stokes equations:

$$\nabla \cdot \mathbf{u} = 0 \tag{2.11a}$$

$$\frac{\partial \mathbf{u}}{\partial t} + \mathbf{u} \cdot \nabla \mathbf{u} = -\frac{1}{\rho}\nabla p + \nu \nabla^2 \mathbf{u} + \mathbf{f}_{body} \tag{2.11b}$$

where $\nu = \frac{\mu}{\rho}$.

2.3 Scalar Transport Equation

The scalar transport is modelled by a diffusion - convection (advection) equation that can be recovered from first principles (mass or energy balance). This describes physical phenomena where particles, energy, or other physical scalar quantities are transferred inside a physical system due to two processes: diffusion and convection. The same equation can also be called the advection-diffusion equation. The general equation is:

$$\frac{\partial c}{\partial t} = \nabla \cdot (D \nabla c) - \nabla \cdot (\mathbf{u} c) + R \tag{2.12}$$

where c is the variable of interest (species concentration for mass transfer, temperature for heat transfer), D is the diffusivity coefficient, R describes ”sources” or ”sinks” of the quantity c. In eq. 2.12 each term have a physical meaning:

- $\nabla \cdot (D \nabla c)$, describes diffusion flux proportional to the gradient;
- $-\nabla \cdot (\mathbf{u} c)$ describes convection (or advection) flux;
- R, describes the creation or destruction of the quantity c.

The diffusion flux is here assumed to follow the Fick's law: this postulates that the flux goes from regions of high concentration to regions of low concentration, with a magnitude that is proportional to the concentration gradient. In particular, the diffusion coefficient D is proportional to the squared fluctuating velocity of the diffusing molecules.

2.4 Dynamic similarity

Similitude is a concept applicable to the testing of engineering models. A model is said to have similitude with the real application if the two share geometric similarity, kinematic similarity and dynamic similarity. The term dynamic similitude is often used as a catch-all because it implies that geometric and kinematic similitude have already been met. The following criteria are required to achieve similitude:

- Geometric similarity means that the model is the same shape as the application, usually at different size (at different scale);
- Kinematic similarity when fluid streamlines are similar;
- Dynamic similarity implies that the ratios of all forces acting on corresponding fluid particles and boundary surfaces in the two systems are the same.

To satisfy and apply the dynamic similarity is necessary to use the dimensional analysis to express the system with as few independent variables and as many dimensionless parameters as possible.
For fluid dynamics, in particular, similarity allows us to relate two flows having different length-scales, flow speed or fluid properties, provided the values of these non-dimensional parameters are comparable.
Dimensional analysis is based on Buckingham theorem which states that if a physical process has "n" variables, with "k" are repeating variables, then there are "n-k"

independent non-dimensional numbers that can describe the process. Applying this theorem to the differential equations it is possible to obtain the non-dimensional parameters that describe the flow.

From the Navier-Stokes equation, balancing inertial and viscous forces, it is possible to obtain the Reynolds number [Kundu P.K.(2004)]:

$$Re = \frac{ul}{\nu} \tag{2.13}$$

In 2.13 equation u represents the typical velocity, l the characteristic length scale and $\nu = \frac{\mu}{\rho}$ the kinematic viscosity. The Reynolds number represents the ratio between inertial and viscous forces: if it is much lower than the unity, the inertial forces can be neglected in comparison with the viscous forces; on the contrary, if the Reynolds number is high, the viscous forces are much smaller than the inertial forces and the approximation of non-viscous flow could be made far from the boundary [Kundu P.K.(2004)]. Moreover th Reynolds number is used to characterize different flow regimes:

- laminar flow occurs at low Reynolds numbers, where viscous forces are dominant, and is characterized by smooth, constant fluid motion;
- turbulent flow occurs at high Reynolds numbers and is dominated by inertial forces, which tend to produce chaotic eddies, vortices and other flow instabilities.

From the scalar equation it is possible deduce others non-dimensional numbers. The first of these is the Schmidt number defined as the ratio of viscosity (ν) and scalar diffusivity (D), and is used to characterize fluid flows in which there are simultaneous momentum and scalar diffusion convection processes:

$$Sc = \frac{\nu}{D} \tag{2.14}$$

From the dimensional analysis of the scalar equation (2.12) another important non-dimensional number appear. This represents the importance of the advective transport rate compared to the diffusive transport rate. This parameter is called Peclet number and is equivalent to the product of the Reynolds number and the Schmidt number:

$$Pe = \frac{ul}{D} = \frac{ul}{\nu}\frac{\nu}{D} = Re\,Sc \tag{2.15}$$

In chapter 3, we analyze the flow in a porous media starting with the equations discussed in this chapter and in chapter 2. The non-dimensional equations that will be obtained for the flow in a porous media (eq. 3.19) have some extra-terms giving another important non-dimensional number: the Darcy number (Da), the ratio of the permeability of the medium and the square of the typical length l,

$$Da = \frac{K}{l^2}. \tag{2.16}$$

with K is the permeability of the medium (see chapter 2).

Chapter 3

Porous Media

In this second chapter the flow dynamics in porous media is presented. Firstly, porous medium is introduced with its definition and some examples of applications. In the second part we present the volume average method, which allows to derive equations to study the fluid dynamics inside a porous medium from a macroscopic perspective. Three equations are obtained with this method (continuity, Navier-Stokes and scalar conservation volume average equations) and they will be used in the simulations of this thesis project. In particular, the scalar equation allows to estimate the mass transfer in a porous medium, that is one of the main goal of this project.

3.1 Introduction to Porous Media

First of all, it is necessary to define the term "porous media". It is quite intuitive to think at a porous media as a "solid with holes", but for example a hollow cylinder would not normally be classed as a porous media. A porous media can be defined more precisely as:

- a portion of space occupied by heterogeneous or multiphase matter. At least

one of the phases comprising this matter is not solid. The solid phase is called the solid matrix. The space within the porous media domain that is not part of the solid matrix is referred to as void spaces.

- The solid phase should be distributed throughout the porous media within the domain occupied by a porous media; solid must be present inside each representative elementary volume.

- At least some of the pores comprising the void space should be interconnected.

However, it is not simple to give an exact definition still sufficiently general to be applied to the wide variety of porous media and for this reason, the definition has to be improved for every different case.

There are a lot of different types of porous media and therefore, there are lots of different applications.

Fluid-filled porous media are ubiquitous in many natural and industrial systems. The working of these systems is controlled and/or affected by the movement of fluids, solutes, particles, electrical charges, and heat through them. Examples of natural porous media and corresponding processes are the flow of oil, gas, and water in oil reservoirs; the potential mobilization of methane in gas hydrates; the flow of Non-Aqueous Phase Liquids (NAPLs) in contaminated aquifers; the storage of CO2, nuclear waste, other hazardous wastes, and heat in the subsurface; the flow of fluids and solutes in biological tissues; and melting and metamorphism of snow. Examples of industrial porous media and corresponding processes are the drying of paper pulp, the adsorption of liquids in diapers and similar absorbing products, gas and water management in fuel cells, and the drying of foods, as well as water and solute movement in building materials, detergent tablets, textiles, foams, coatings, paper, and filters. Many physical, chemical, thermal, and biological pro-

cesses (such as fluid flow, diffusion, capillarity, dissolution, adsorption, clogging, degradation, shrinkage, swelling, fracturing, and flow of electrical charges) occur in these materials. For the design, operation, and maintenance of porous media systems, it is extremely important to understand these processes, describe them quantitatively (by mathematical models) and simulate them [Bear(1972)].

Also in aerospace engineer porous media are encountered. In fact, modern demands for increasingly efficient energy delivery and the anticipated demand for renewable energy have generated considerable interest in energy storage technologies. One of the most compelling of such technologies are the redox-flow battery (RFB) and fuel cells. There are currently several types of these devices under development, each employing different redox couples: one of the most popular types is the all-vanadium redox battery. These applications use porous carbon electrodes and porous membranes. The bottleneck for the peak performance of these batteries is due to the relatively slow mass transport occurring in the porous media. Enhancing the mixing and mass transfer in these media is then crucial

[You *et al.*(2009)You, Zhang & Chen, Shah *et al.*(2008)Shah, Watt-Smith & Walsh].

3.2 Volume Average Method

The fluid dynamic equations that we have discussed in chapter 1 are still valid in porous media but they are difficult to apply to porous media due to the complex shape of the void spaces. For example, in the process of drying a porous medium, one needs to know how water is transported through the pores to the external surface where it is removed by warm, dry air. The direct analysis of this process, in terms of transport equations that are valid within the pores, is essentially impossible because of the complex structure of the typical porous medium.

The method of volume averaging is a technique that can be used to rigorously de-

rive continuum equations for multiphase systems. This means that equations which are valid within a particular phase can be spatially smoothed to produce equations that are valid everywhere, but at a macroscopic level. Rather than attacking that problem in terms of equations and boundary conditions that are valid in the pores, we can use the pore-scale information to derive local volume averaged equations that are valid everywhere (for an application example see
[Hussong *et al.*(2011)Hussong, Breugem & Westerweel]).
Given these equations, the problem can be solved using classical methods.
Porous medium can be sketched as in fig. 3.1 and in fig.3.2

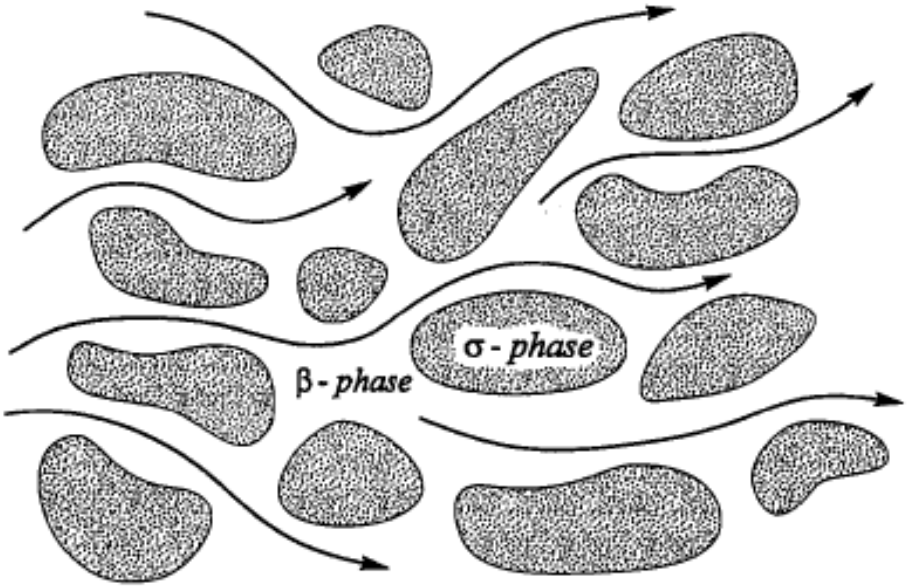

Figure 3.1: Flow in a porous media. From [Whitaker(1996)]

It is necessary to define the following quantities, where β is the liquid phase and σ the solid phase:

- $\mathscr{A}_{\beta\sigma}$ interfacial area of the $\beta - \sigma$ interface contained whitin the macroscopic systems

- $\mathscr{A}_{\beta e}$ area of entrances and exits for the β-phase contained whitin the macro-

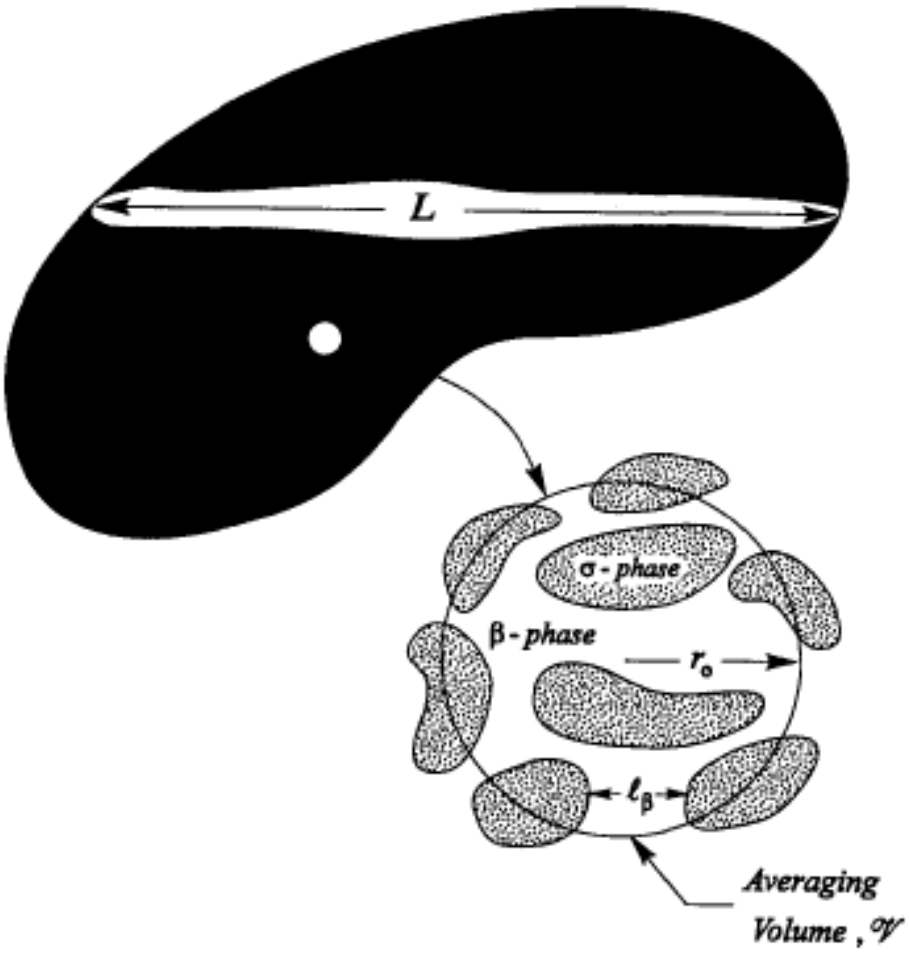

Figure 3.2: Macroscopic region and local averaging volume. From [Whitaker(1996)]

scopic systems

- $A_{\beta\sigma}$ interfacial area of the $\beta - \sigma$ interface contained whitin the averaging volume
- l_β characteristic length for the β-phase
- L characteristic length for macroscopic quantities
- $\mathbf{n}_{\beta\sigma}$ unit normal vector directed from the β-phase toward the σ-phase
- $\mathscr{V}$ local averaging volume
- V_β volume of the β-phase contained within the averaging volume
- $\mathbf{v}_\beta$ velocity in the β-phase

There are two types of volume averages that are commonly encountered in the study of multiphase transport phenomena. For some function ψ_β associated with the β-phase, the superficial average is defined by:

$$\langle \psi_\beta \rangle = \frac{1}{\mathscr{V}} \int_{V_\beta} \psi_\beta dV \tag{3.1}$$

The second type of volume average is the intrinsic average that is defined according to:

$$\langle \psi_\beta \rangle^\beta = \frac{1}{V_\beta} \int_{V_\beta} \psi_\beta dV \tag{3.2}$$

These two averages are related by:

$$\langle \psi_\beta \rangle = \varepsilon \langle \psi_\beta \rangle^\beta \tag{3.3}$$

where ε_β is the volume fraction of the β-phase defined as

$$\varepsilon_\beta = \frac{V_\beta}{\mathscr{V}}. \tag{3.4}$$

In other words, ε_β represents the porosity, i.e. the ratio between the void volume and the total volume. When $\varepsilon_\beta = 1$, everything is void space, and when $\varepsilon_\beta = 0$ the volume is all occupied by the solid phase. Obviously, ε_β depends of the volume quantity under examination, for example in some regions it could be only 0 or only 1, but it is possible to show that if the porosity is averaged on a scale large enough, it has a constant value, as shown if fig. 3.3. [Whitaker(1999)] and [Bear(1972)]

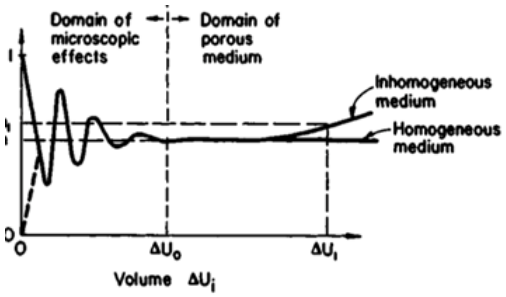

Figure 3.3: Representative elementary volume of porosity. From [Bear(1972)]

To apply the Volume Average Method to fluid dynamic equations it is necessary to also make the average of a gradient. This problem has been solved by [Howes & Whitaker(1985)] and their result is the averaging theorem:

$$\langle \nabla \psi_\beta \rangle = \nabla \langle \psi_\beta \rangle + \frac{1}{\mathscr{V}} \int_{A_{\beta\sigma}} \mathbf{n}_{\beta\sigma} \psi_\beta dA \tag{3.5}$$

3.2.1 Continuity Equation

The averaging process can be applied to the continuity equation to obtain

$$\frac{1}{\mathscr{V}} \int_{V_\beta} \nabla \cdot \mathbf{v}_\beta dV = \langle \nabla \cdot \mathbf{v}_\beta \rangle = 0 \tag{3.6}$$

Applying the averaging theorem (3.5), the continuity equation becomes

$$\langle \nabla \cdot \mathbf{v}_\beta \rangle = \nabla \cdot \langle \mathbf{v}_\beta \rangle + \frac{1}{\mathscr{V}} \int_{A_{\beta\sigma}} \mathbf{n}_{\beta\sigma} \cdot \mathbf{v}_\beta dA = 0 \tag{3.7}$$

Where $\langle \mathbf{v}_\beta \rangle$ is the superficial average velocity. Since the solid phase is impermeable, this result simplifies to

$$\nabla \cdot \langle \mathbf{v}_\beta \rangle = 0 \tag{3.8}$$

This equation shows that the superficial average velocity is solenoidal. It's possible also to deduce the continuity equation in terms of the intrinsic average velocity $\langle \mathbf{v}_\beta \rangle^\beta$ using the relation between the two types of average (intrinsic and superficial) and this is given by

$$\nabla \cdot (\varepsilon_\beta \langle \mathbf{v}_\beta \rangle^\beta) = 0 \tag{3.9}$$

3.2.2 Momentum Equation

The superficial average of the Navier-Stokes equations can be expressed as

$$\langle \rho_\beta \frac{\partial \mathbf{v}_\beta}{\partial t} \rangle + \langle \rho_\beta \mathbf{v}_\beta \cdot \nabla \mathbf{v}_\beta \rangle = -\langle \nabla p_\beta \rangle + \langle \rho_\beta \mathbf{g} \rangle + \langle \mu_\beta \nabla^2 \mathbf{v}_\beta \rangle \tag{3.10}$$

where ρ_β , p_β and μ_β are respectively density, total pressure and viscosity of the β-phase. Ignoring the variations of ρ_β (incompressible flows), requiring that the variations of μ_β be negligible whitin the averaging volume, imposing the following length-scale constrains $l_\beta \ll r_0$, $r_0^2 \ll L^2$ and lastly ignoring the lower-order terms the Navier-Stokes equation can be rewritten with intrinsic average velocity as:

$$\begin{aligned}
&\rho_\beta \frac{\partial \langle \mathbf{v}_\beta \rangle^\beta}{\partial t} + \rho_\beta \langle \mathbf{v}_\beta \rangle^\beta \nabla \cdot \langle \mathbf{v}_\beta \rangle^\beta + \rho_\beta \varepsilon_\beta^{-1} \nabla \cdot \langle \widetilde{\mathbf{v}}_\beta \widetilde{\mathbf{v}}_\beta \rangle \\
&= -\nabla \langle p_\beta \rangle^\beta + \rho_\beta \mathbf{g} + \mu_\beta (\nabla^2 \langle \mathbf{v}_\beta \rangle^\beta + \\
&+ \varepsilon_\beta^{-1} \nabla \varepsilon_\beta \cdot \nabla \langle \mathbf{v}_\beta \rangle^\beta + \varepsilon_\beta^{-1} \langle \mathbf{v}_\beta \rangle^\beta \nabla^2 \varepsilon_\beta) + \\
&+ \frac{1}{V_\beta} \int_{A_{\beta\sigma}} \mathbf{n}_{\beta\sigma} \cdot (-\mathbf{I} \widetilde{p}_\beta + \mu_\beta \nabla \widetilde{\mathbf{v}}_\beta) dA,
\end{aligned} \tag{3.11}$$

where the terms $\widetilde{\mathbf{v}}_\beta$ and $\widetilde{p}_\beta$ are the spatial deviation velocity and spatial deviation pressure obtained using the decomposition given by Gray (1975)

$$\mathbf{v}_\beta = \langle \mathbf{v}_\beta \rangle^\beta + \widetilde{\mathbf{v}}_\beta \tag{3.12}$$

Further, one needs to model some terms in that equation (3.11) to obtain a closed form. From [Whitaker(1999)] and [Whitaker(1996)] it is possible to re-write the integral term as

$$\frac{1}{V_\beta} \int_{A_{\beta\sigma}} \mathbf{n}_{\beta\sigma} \cdot (-\mathbf{I}\widetilde{p}_\beta + \mu_\beta \nabla \widetilde{\mathbf{v}}_\beta) dA = -\mu_\beta \varepsilon_\beta \mathbf{K}_\beta^{-1} \langle \mathbf{v}_\beta \rangle^\beta - \mu_\beta \varepsilon_\beta \mathbf{K}_\beta^{-1} \mathbf{F} \langle \mathbf{v}_\beta \rangle^\beta \tag{3.13}$$

where $\mathbf{K}_\beta$ is the permeability tensor. If the porous media is isotropic the tensor becomes spheric, $\mathbf{k}_\beta = k\mathbf{I}$, and characterized only by a single scalar quantity: The permability k. The scalar permeability has the dimension of a length squares and can be approximated by the semi-empirical formula (valid for porous media of spheres)

$$k = \frac{1}{180} \left(d_p\right)^2 \frac{\varepsilon^3}{(1-\varepsilon)^2}, \tag{3.14}$$

with d_p the pore size. The corresponding dimensionless number is the Darcy number with is defined as $Da = k/l^2$ with l a characteristic macroscopic length. $\mathbf{F}$ is the Forchhemeir Correction and can be experimentally shown [Whitaker(1996)]

$$F_0 = \frac{\varepsilon_\beta}{100(1-\varepsilon)} \frac{\rho_\beta \langle \mathbf{v}_\beta \rangle^\beta d_p}{\mu_\beta}. \tag{3.15}$$

Another modification it is necessary to simplify the term with spatial deviation velocity $\widetilde{\mathbf{v}}_\beta$. In Whitaker [Whitaker(1996)] it is explained how to get $\widetilde{\mathbf{v}}_\beta = \mathbf{M} \cdot \langle \mathbf{v}_\beta \rangle^\beta$, with $\mathbf{M} = -\mathbf{I}$ where $\mathbf{I}$ is the identity matrix.

So,

$$\nabla \cdot \langle \widetilde{\mathbf{v}}\widetilde{\mathbf{v}} \rangle = \nabla \cdot (\langle \mathbf{v}_\beta \rangle^\beta \cdot \mathbf{M}^T \mathbf{M} \cdot \langle \mathbf{v}_\beta \rangle^\beta) \tag{3.16}$$

At the end, one can obtain an alternative form of continuity equation (3.9)

$$\nabla \cdot \langle \mathbf{v}_\beta \rangle^\beta = -\frac{1}{\varepsilon_\beta} \nabla \varepsilon_\beta \cdot \langle \mathbf{v}_\beta \rangle^\beta \tag{3.17}$$

and transform the term with spatial deviation velocity (3.16) into

$$\nabla \cdot \langle \widetilde{\mathbf{v}}\widetilde{\mathbf{v}} \rangle = (\nabla \varepsilon_\beta \cdot \langle \mathbf{v}_\beta \rangle^\beta) \langle \mathbf{v}_\beta \rangle^\beta \tag{3.18}$$

Finally, the dimension-less Volume Average Navier-Stokes for the momentum balance can be rewritten as

$$\begin{aligned} &\frac{\partial \langle \mathbf{v}_\beta \rangle^\beta}{\partial t} + \langle \mathbf{v}_\beta \rangle^\beta \nabla \cdot \langle \mathbf{v}_\beta \rangle^\beta = -\nabla \langle p_\beta \rangle^\beta + \mathbf{g} + \frac{1}{Re} \nabla^2 \langle \mathbf{v}_\beta \rangle^\beta \\ &- \frac{1}{\varepsilon_\beta} (\nabla \varepsilon_\beta \cdot \langle \mathbf{v}_\beta \rangle^\beta) \langle \mathbf{v}_\beta \rangle^\beta + \frac{1}{\varepsilon_\beta} \frac{1}{Re} \nabla \varepsilon \cdot \nabla \langle \mathbf{v}_\beta \rangle^\beta \\ &+ \frac{1}{Re} \frac{1}{\varepsilon} \nabla^2 \varepsilon - \frac{1}{Re} \frac{F_0}{Da} \varepsilon_\beta \langle \mathbf{v}_\beta \rangle^\beta - \frac{1}{Re} \frac{\varepsilon_\beta}{Da} \langle \mathbf{v}_\beta \rangle^\beta \end{aligned} \tag{3.19}$$

3.2.3 Scalar equation

The same volume-average process can be applied to the scalar equation (2.12) to obtain the following equation (without any sources of scalar value and with intrinsic average velocity)

$$\varepsilon_\beta \frac{\partial \langle c_\beta \rangle^\beta}{\partial t} + \nabla \cdot \left[\varepsilon_\beta \langle \mathbf{v}_\beta \rangle^\beta \langle c_\beta \rangle^\beta \right] = \nabla \cdot \left[\varepsilon \mathbf{D}_e \cdot \nabla \langle c_\beta \rangle^\beta \right] \tag{3.20}$$

where

- c_β is the scalar value in the β-phase
- $\langle c_\beta \rangle^\beta$ is the intrinsic average of the scalar value in the β-phase

- $\mathbf{D}_e$ is the effective diffusivity tensor which depends on the fluid and porous media structure.

The total mass flux is defined by $\mathbf{F}$

$$\varepsilon_\beta \frac{\partial \langle c_\beta \rangle^\beta}{\partial t} + \nabla \cdot \mathbf{F} = 0. \tag{3.21}$$

At steady state (time dependent terms equal to 0), the total flux is equal to

$$\mathbf{F} = \varepsilon \mathbf{D}_e \cdot \nabla \langle c_\beta \rangle^\beta - \varepsilon_\beta \langle \mathbf{v}_\beta \rangle^\beta \langle c_\beta \rangle^\beta \tag{3.22}$$

This flux equation will be used to analyze the mass flux inside a porous medium using the data of our simulations.

Chapter 4

Numerical approach

This third chapter is dedicated to present the methodology used to solve fluid dynamics problems applied to porous media. The first part introduces the Computational Fluid Dynamics (CFD), the discipline whose aim is to solve numerically the equations governing a fluid in motion. A particular subsection is dedicated to the spectral element method, which is the numerical technique used on NEK5000 code that is an open source tool developed at Argonne National Laboratories, USA. The second part focuses on the new implementation added to the code during this thesis project. Nek5000 is actually a fluid solver written for the Navier-Stokes equations for a single-phase flow. The extra terms due to the volume average method to deal with a porous medium have been added to the code. The last section introduces the functions chosen to prescribe the local porosity in the medium.

4.1 Introduction to CFD

As it has already been discussed in Chapter 1, computational fluid dynamics (CFD) is a branch of fluid mechanics that uses numerical analysis and computer algorithms to solve and analyze problems that involve fluid flows. It is necessary to

solve the fluid dynamics equations with numerical methods because they usually do not have closed-form solutions.

During prepocessing:

- the geometry (physical bounds) of the problem is defined;
- the volume occupied by the fluid is divided into discrete cells (mesh);
- the physical model is defined;
- the boundary conditions are defined.

Later, the simulation is started and the equations are solved iteratively and finally a post-processor is used for the analysis and visualization of the resulting solution. Depending on the method of choice (the numerical analysis part) and the given resolution (the computing part), the difference between the numerical solution and the true solution will vary.

The choice of the discretization method is then very important. Some of the discretization methods used are:

- Finite difference method (FDM);
- Finite Volume Method (FVM);
- Finite Element Method (FEM);
- Spectral Element Method (SEM).

The first method uses finite difference equations to approximate the derivatives. The other two methods involve the partition of the whole domain into simpler parts, called Finite Volumes or Finite Elements, and the calculation of the fluid velocity at discrete places of these sub-domains. The last one, Spectral Element Method is a formulation of the Finite Element Method that uses high degree polynomials as base functions.

4.1.1 Spectral Element Method

The Spectral Element Method is capable of combining the accuracy of the Fourier spectral methods and the flexibility of methods based on low-order local approaches. It is a high-order weighted residual technique similar to FEM, but based on orthogonal polynomials and highly accurate numerical quadrature. The original implementation by Patera (1984) was based on Chebyshev polynomials, but later implementations have rather been utilizing Legendre polynomials. The method exhibits several favourable computational properties, such as the use of tensor products and naturally diagonal mass matrices, which makes it suitable for parallel implementations and large calculations [Malm(2011)].

4.2 Nek5000 new implementation

Nek5000 is an open-source computational fluid dynamics solver based on the spectral element method. The code is written in Fortran77/C and employs the MPI standard for parallelism.

In this project, Nek5000 is the software used to solve fluid dynamics equation inside a porous medium.

In the following section, we describe the additions and changes to the original code. In particular, Nek5000 has already implemented the Continuity, Navier-Stokes and Scalar equations for single-phase flows and so it will be shown how to derive the extra terms due to presence of the porous medium (volume average method), and add them to the original code.

In the following section, to make the notation simpler, we use $\mathbf{v}$ for the intrinsic average velocity $\langle \mathbf{v}_\beta \rangle^\beta$, with ε to the volume fraction of β-phase ε_β and with c the intrinsic average concentration of the scalar in the β-phase$\langle c_\beta \rangle^\beta$. In all the implemented equations it is assumed a local homogeneity and isotropy of the porous

media.

[Paul F. Fischer & Kerkemeier(2008)]

4.2.1 Continuity equation

Expanding the volume averaged continuity equation (3.9), we have:

$$\nabla\varepsilon \cdot \mathbf{v} + \varepsilon(\nabla \cdot \mathbf{v}) = 0 \tag{4.1}$$

The extra term to add to the continuity equation is the term on the right hand side:

$$\nabla \cdot \mathbf{v} = \underbrace{-\frac{1}{\varepsilon}(\nabla\varepsilon \cdot \mathbf{v})}_{} \tag{4.2}$$

In the Nek5000 code it has been written in components as:

$$\frac{\partial \mathbf{u}}{\partial x} + \frac{\partial \mathbf{v}}{\partial y} + \frac{\partial \mathbf{w}}{\partial z} = \underbrace{-\frac{1}{\varepsilon}\left(\frac{\partial \varepsilon}{\partial x}\mathbf{u} + \frac{\partial \varepsilon}{\partial y}\mathbf{v} + \frac{\partial \varepsilon}{\partial z}\mathbf{w}\right)}_{}. \tag{4.3}$$

This new part has been implemented in the routine turbochannel.f .

4.2.2 Scalar equation

The mass transfer equation (3.20) can be expressed as

$$\frac{\partial c}{\partial t} + \mathbf{v} \cdot \nabla c = D_e \nabla^2 c + \frac{1}{\varepsilon}\nabla(\varepsilon D_e) \cdot \nabla c \tag{4.4}$$

where $D_e = \varepsilon^{3/2} D$ is the effective diffusivity modeled using the Bruggemann correction and D is the constant diffusivity. Further this equation can be written as

$$\frac{\partial c}{\partial t} + \mathbf{v} \cdot \nabla c = D\nabla^2 c + \underbrace{D(\varepsilon^{3/2} - 1)\nabla^2 c + \frac{D}{\varepsilon}\nabla(\varepsilon^{5/2}) \cdot \nabla c}_{} \tag{4.5}$$

highlighting the term to add in the code. This equation can be rewritten in non-dimensional form and in components as

$$\frac{\partial c}{\partial t}+\mathbf{v}\cdot\nabla c = \frac{1}{Pe}\nabla^2 c+\underbrace{\frac{1}{Pe}(\varepsilon^{3/2}-1)\nabla^2 c + \frac{5}{2}\frac{1}{Pe}\sqrt{\varepsilon}\left(\frac{\partial \varepsilon}{\partial x}\frac{\partial c}{\partial x}+\frac{\partial \varepsilon}{\partial y}\frac{\partial c}{\partial y}+\frac{\partial \varepsilon}{\partial z}\frac{\partial c}{\partial z}\right)}_{} \quad (4.6)$$

4.2.3 Navier-Stokes equation

From the Volume Average Navier-Stokes equation (3.19), the extra term added in the Nek5000 code is as below:

$$\begin{aligned}&\frac{\partial \mathbf{v}}{\partial t}+\mathbf{v}\nabla\cdot\mathbf{v} = -\nabla p+\mathbf{g}+\frac{1}{Re}\nabla^2\mathbf{v}\\ &\underbrace{-\frac{1}{\varepsilon}(\nabla\varepsilon\cdot\mathbf{v})\mathbf{v}+\frac{1}{\varepsilon}\frac{1}{Re}\nabla\varepsilon\cdot\nabla\mathbf{v}-\frac{1}{Re}\frac{F_0}{Da}\varepsilon|\mathbf{v}|\mathbf{v}+\frac{1}{Re}\left[\frac{1}{\varepsilon}\nabla^2\varepsilon-\frac{\varepsilon}{Da}\right]\mathbf{v}}_{}\end{aligned} \quad (4.7)$$

where it is assumed

$$F_0 = \frac{\varepsilon_\beta}{100(1-\varepsilon)}Re_p \quad (4.8)$$

with Re_p the porous scale Reynolds number.

4.2.4 Routine Added in the code

Nek5000 has already implemented the fluid dynamics equations, so it was necessary to add the extra terms found in the previous sections in the continuity,scalar and momentum equations due to the volume averaging method for a porous medium. Besides, it has been necessary to choose porosity function and compute its first and second derivatives.

To analyze the results, routines have been written to average on every x-z plane (planes parallel to the wall of the infinite channel) and on the entire volume. Planar average routine has been applied to the velocity in y-direction (wall normal), scalar, derivative in y direction of the scalar, convection, diffusion, flux and diver-

gence. Volume average has been applied to velocity, scalar and derivatives to study mixing in time (chapter 5) .

Some of these values have been used only for debugging purposes.

Different types of output files for analyzing the simulation data with Matlab or to create graphics for a better understanding have been also developed.

4.3 Porous Function

The goal of this project, as already said, is to evaluate the mixing of a fluid that flows inside a porous media of variable porosity. For this reason, one of the most important parts of this project is the choice of a porosity distribution. This has been prescribed using a function which gives a specific value of the volume fraction of liquid phase ε_β in every points. There are endless possibility to create different "porous functions" (see as example [Kee & Gavriilidis(2008)]) but in this case, it is necessary to create a function which satisfies some restrictions.

First of all, it has to be time independent and space dependent, so that in every point of the channel it assumes different values but always between 0 and 1 corresponding to pure solid and void.

In the simulations, the boundary conditions imposed are periodic in x and z directions (streamwise and spanwise directions) and so, the porous function has to be periodic in these directions. The porous function values created are around the bulk value, i.e. 0.7 ± 0.2 . The value are not near 0 because, in that case, there would not be too much solid volume in that zone and there would be any flow.

Different functions have been created to represent the porous medium distribution inside the channel with different mathematical functions, for example with sin, cosh, tanh etc. It has been decided to show the results only of the "sin function" because it is simple, periodic, with parameters easy to change, derivable in all the

domain and it creates velocity in y and z directions from an originally flow only in x direction. It will be explained in the following chapters that to increase the mixing, and so to increase the flux in the wall normal direction, it is really important to generate flow velocity in that direction.

The "sin function" equation which represent the porosity inside the channel is:

$$\varepsilon(x, y, z) = \varepsilon_c + \Delta\varepsilon \sin(k_x x) \sin(k_y y) \sin(k_z z). \tag{4.9}$$

The parameter ε_c allows to assign the porosity mean value in the plane x-z and $\Delta\varepsilon$ the maximum variation of the porosity in the medium. The others parameters k_x, k_y, k_z define the wave numbers of the periodic function in each direction. Examples of the different variable porosities are shown in figures 4.1 to 4.4.

The first two images 4.1 and 4.2 refer to 2D porous function, where porosity is constant in the z direction. Figs. 4.3 and 4.4 refer to 3D porous functions with different periodicity than in the previous examples.

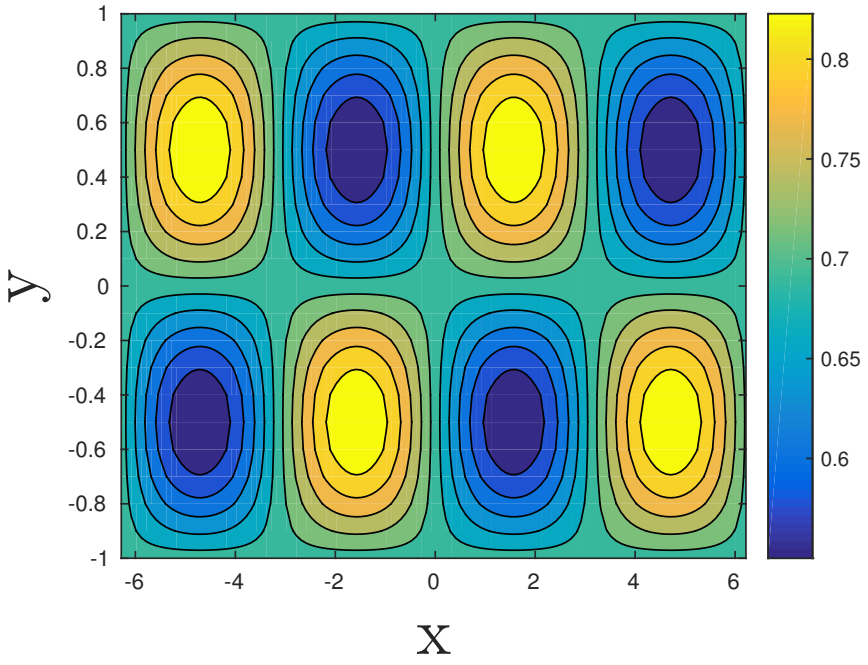

Figure 4.1: Porosity values in XY plane. Ky=2pi , Kx=1

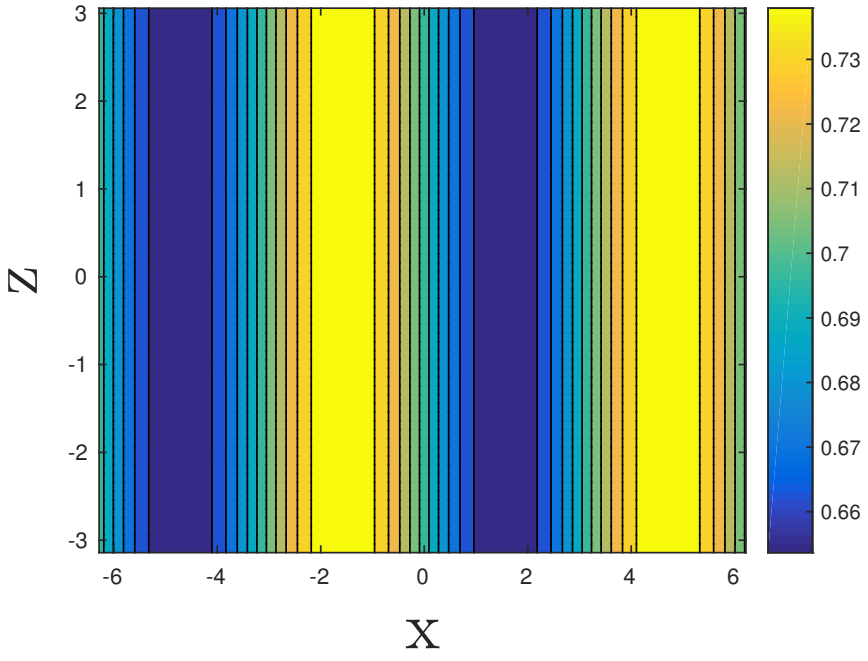

Figure 4.2: Porosity values in XZ plane. Ky=2pi , Kx=1

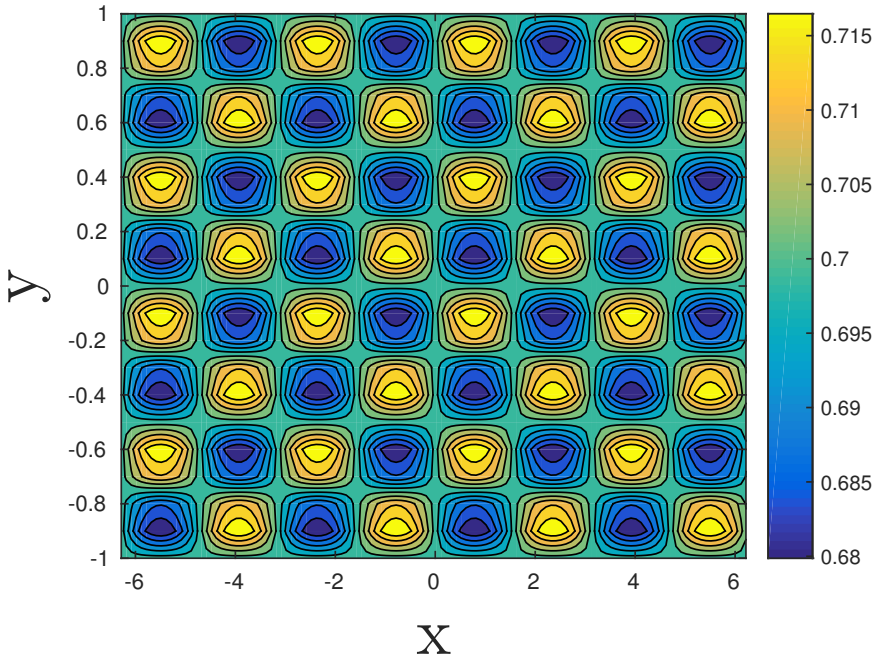

Figure 4.3: Porosity values in XY plane. Ky=2pi , Kx=1 , Kz=1

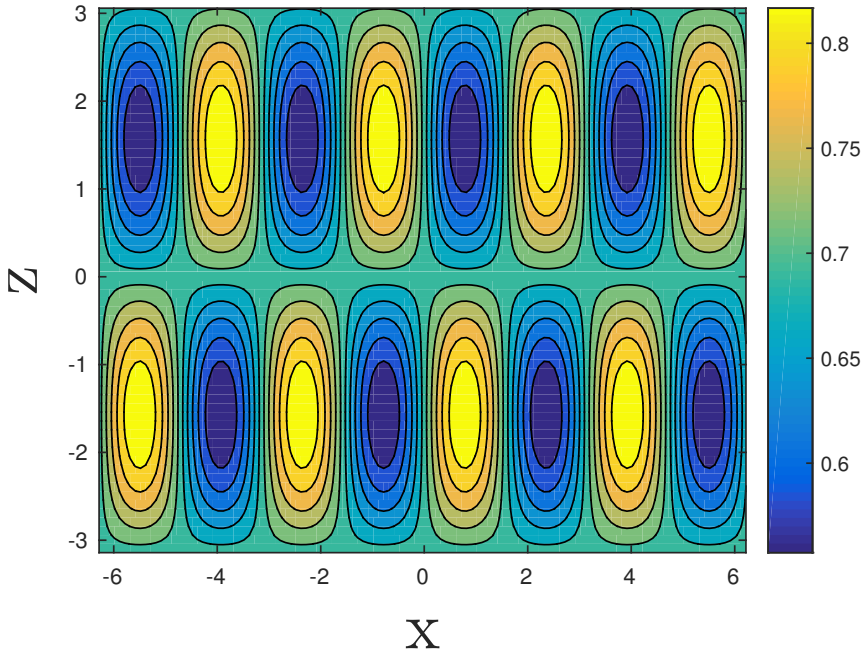

Figure 4.4: Porosity values in XZ plane. Ky=2pi , Kx=1 , Kz=1

Chapter 5

Results

This chapter is dedicated to the discussion of the results obtained by the numerical simulations carried out during this project. In the first section the set-up of the simulations is fully described. In the second section the results are shown with the following order: firstly the velocity fields, scalar field and the different total flux obtained are displayed for the 2D simulations. Then the same quantities are shown for the case with a 3D porosity distribution. Finally, the focus is on the analysis of the results to understand the parameters that influence the results.

5.1 Simulation set-up

5.1.1 Dimensionless numbers of the problem

In order to select the typical dimension-less numbers used in the present project we refer to the flows found in Fuel Cells and Redox Flow Battery applications. These parameters will be kept fixed varying only the distribution of the porosity to assess its effect on mixing. The flow in these electrodes can be sketched as a parallel channel flow in a porous media. The flow shows bulk velocities in the range $u_b \simeq 10^{-3} \div 10^{-1} ms^{-1}$, the typical thickness is $H = 10^{-3} \div 10^{-2} m$ and the

kinematic pure fluid viscosity is $\nu \simeq 10^{-6} \div 10^{-5} m^2 s^{-1}$ (water or air solutions), so the value of the Reynolds number ranges in $Re = \frac{u_b H}{\nu} = 1 \div 1000$ (eq. 2.13). We fix this number to $Re = 100$ for all simulations to be in the range. The Peclet number range is very wide: $Pe = \frac{u_b H}{D} = 1 \div 10^6$ where $D \simeq 10^{-5} \div 10^{-9}$ is the mass diffusion coefficient. We chose Peclet number $Pe = 10$ in order to keep relatively fast the simulation time.

Concerning the porous media properties we fixed the bulk porosity to $\epsilon = 0.7$ modulating the local value with prescribed harmonic functions as previously described. The Darcy number defined in eq. (3.14) is a function of the porosity distribution and so, its value is not fixed as the other adimensional numbers, but changes across the channel. However, we fixed the ratio between the typical pore size to the channel height to be $d_p/H = 0.025$. This choice is consistent with a porous media constituted by fibers of $d_p \simeq 100\mu m$. Tab. 5.1 shows the list of dimensionless parameters used in all the simulations done.

Dimensionless parameters	$\overline{\varepsilon}$	$\Delta\varepsilon$	Re_b	Pe	Sc	d_p/H
Values	0.7	0.2	100	10	0.1	0.025

Table 5.1: List of dimensionless parameters used in all the simulations

5.1.2 Simulation parameters

The flow geometry is constituted by a parallel channel flow for all cases. Hereafter all the quantities are made dimensionless with the bulk velocity u_b, the half-channel width $h = H/2$ and the fluid density ρ and kinematic viscosity ν. The domain sizes is Lx = 2π, Ly = 2 and Lz = 2π in the streamwise, wall-normal and spanwise directions respectively. As usual in channel flow simulation, periodic boundary conditions are imposed to the surface perpendicular to the streamwise (x direction) and spanwise (z direction) for the fluid velocity and the mass transport. Prescrib-

ing periodic boundary conditions (PBC) means that any fluid particle that leaves the simulation box by, say, the right-hand face, re-enters the simulation box by the left-hand face. PBC are used to avoid problems with boundary effects caused by domain finite size. No slip condition for the velocity is imposed on the upper and lower walls (perpendicular to the wall normal direction). The no slip conditions means that the fluid has zero velocity relative to the boundary. Lastly, Dirichlet boundary conditions for the mass concentration are applied at the upper and lower surfaces, where the mass value imposed is equal to 0 at the lower surface and 1 at the upper surface. Only for simulations where the porosity is modulated in the streamwise direction with wave number smaller than one the domain is extended accordingly to maintain the periodicity.

The volume flow rate is constant fixing the bulk velocity to 1. The channel is completely filled with porous medium and the function that describes the variable porosity distribution has been introduced in section 4.3. This function has been formulated to have a constant mean value of porosity in every x-z plane (perpendicular to the wall normal direction) equal to 0.7.

5.1.3 Numerical parameters

The numerical algorithm uses spectral elements to solve the equations.

The mesh of the channel is composed of 8 elements in each direction. The elements of the mesh are not equidistant along wall normal direction because the problem requires increased mesh accuracy near the upper and lower walls. In the streamwise and spanwise directions, however, the elements are equispaced. The interpolating polynomial order for every element of the mesh is 6. The initial condition for the scalar value is a linear distribution of the mass concentration value along the wall normal directions with 0 on the lower surface and +1 on the upper surface; the velocity is null in the y and z directions and parabolic in the streamwise direction.

The total time of each simulation depends on when the flow arrives at the steady-state condition.

5.2 Flow and mass transport analysis

In this first part of the analysis, we do not show all the results of all the simulations done, but only some examples useful to understand the phenomena involved. This discussion is divided into three parts: first, results of 2D simulations, second, the 3D simulations and last, we discuss the effect on the mass transfer providing an interpretation of the results. For both 2D and 3D simulations we display the velocity and scalar fields, the mean scalar value along the wall normal direction y. All the results are taken at steady-state conditions.

5.2.1 2D simulation

Figures 5.1(a) and 5.1(b) show the streamwise x-velocity and wall-normal y-velocity fields for the porous function (4.9) characterized by ky=π and kx=1. These wave numbers of the porosity function imply that we have only one period in both directions. It is possible to see that the velocity fields have the same behavior of the porosity function, and in fact, they have the same number of periods (compare figs. 5.1(a) and 5.2). Another example, it is reported in figures 5.3(a) and 5.3(b) where the velocity field is reported for the porosity function with ky=4π and kx=2 with two periods in streamwise and four periods in wall normal direction. Also in this case, the velocity fields have the same behavior as the variation of the porosity. This trend is true for all the cases studied. The modulation of the porosity field induces a strong change of the flow field whose streamwise velocity strongly differ from the parabola of the uniform porosity case. Significant wallnormal flow velocities also appear that are absent in the reference case.

The highest values of x-velocity are where the porosity values are higher and the highest values of y-velocity are in the middle of every semi-period where the streamlines are more deflected, as shown in fig 5.4(a) and 5.4(b). Stagnant flow appears where the porosity is low.

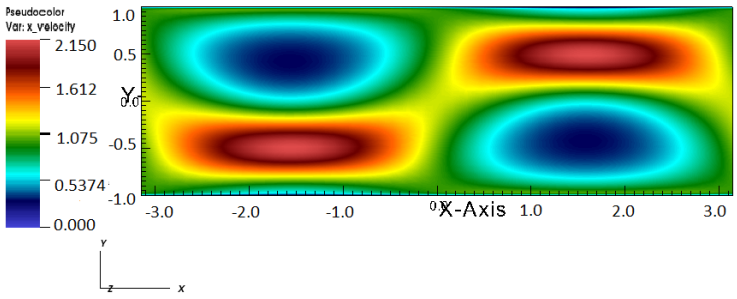

(a)

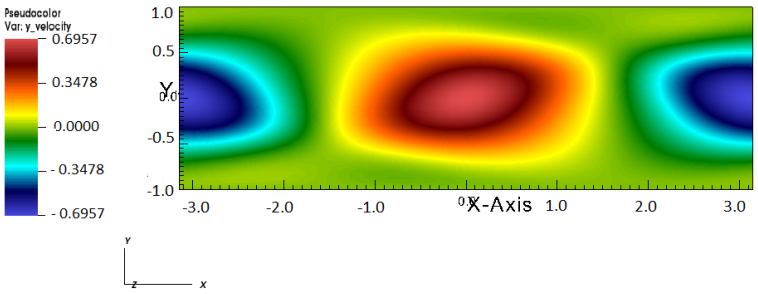

(b)

Figure 5.1: a) streamwise x-velocity, b) wallnormal y-velocity for a porosity distribution with ky=π, kx=1.

The strong change in the flow field clearly affects the mass transport across the channel. The mass concentration fields, with the same porosity functions of the previous examples, are shown in fig.5.5(a) and 5.5(b). It appears from these images that with lower frequency in wall normal direction (ky), a lower number of undulations is obtained, but with higher amplitude.

Being the mass concentration a passive scalar the scalar field is controlled by the corresponding velocity field and number of waves and their period are indeed proportional to ky and kx, respectively. This change in the resultant concentration field

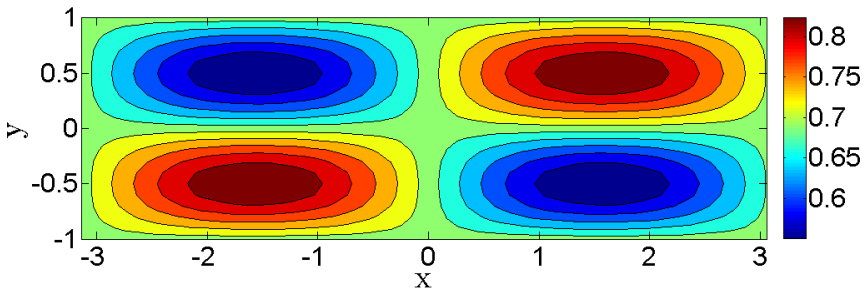

Figure 5.2: Porosity distribution in plane perpendicular to spanwise direction. Ky=pi and Kx=1.

clearly affects the overall mass transport as it will be shown in the following.

In fig. 5.6 the mean value of the mass concentration averaged on each x-z plane along the wall normal direction is shown for the simulations with kx=1 and different wall-normal wave numbers. The results for different ky porosity modulation are compared to the reference case with constant uniform porosity (green line). The case with lower ky, i.e. ky=π, shows the most different profile among the others with respect to the reference case. This case will also show the higher mixing. When the frequency of the modulation is increased in the wall normal direction, the scalar profile looks more similar to the constant porosity case, i.e. the linear profile.

Another important observation is what happens near the upper and the lower wall. In these zones the fluid velocity is vanishing and the flux is controlled mainly by the diffusion term, which is directly proportional to the derivative of the mass concentration along the wallnormal y direction. We note that the slope for the cases with lower modulation frequency in the wall-normal direction ky=π and ky=2π is

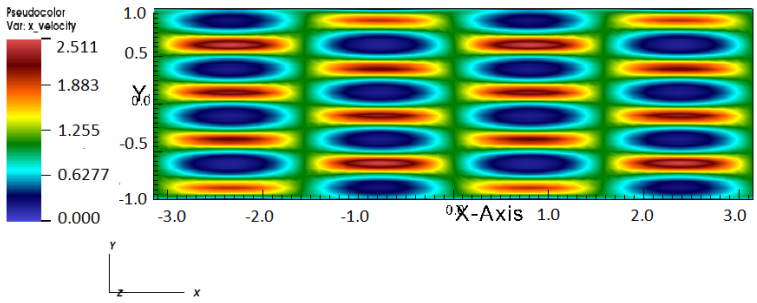

(a)

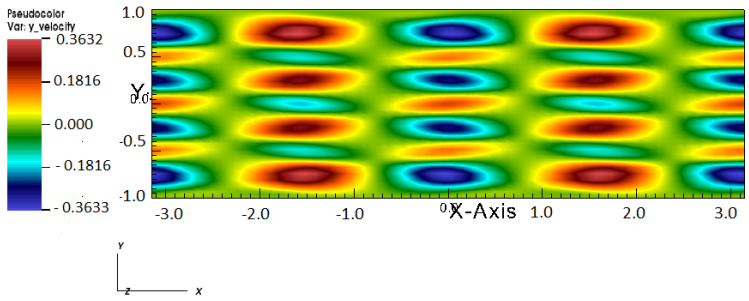

(b)

Figure 5.3: a) Streamwise x-velocity, b) Wallnormal y-velocity for a porosity distribution with ky=π, kx=1.

higher than the reference case indicating enhanced transport. On the other hand, the fluxes when ky=4π and ky=6π have lower slope at the wall than the reference uniform porosity case (green line) and so, lower overall flux.

Now we will discuss the overall flux of all the cases that have been reported in table 5.2. To better discuss the results on the overall mass flux we first fix the streamwise modulation of the porosity to kx=0.5 and kx=1 varying the wallnormal modulation ky, see fig. 5.7(a) and 5.7(b). Here, the vertical axis represents the mass flux normalized by the reference case with uniform porosity, so it is easy to understand how much the mass transfer is enhanced or reduced. From these cases is clear that the flux obtained with null velocity (red line) is always lower than the flux due to the constant porosity function (black line). This means that, without any flow, by modulating the porosity from a constant shape to a sinusoidal

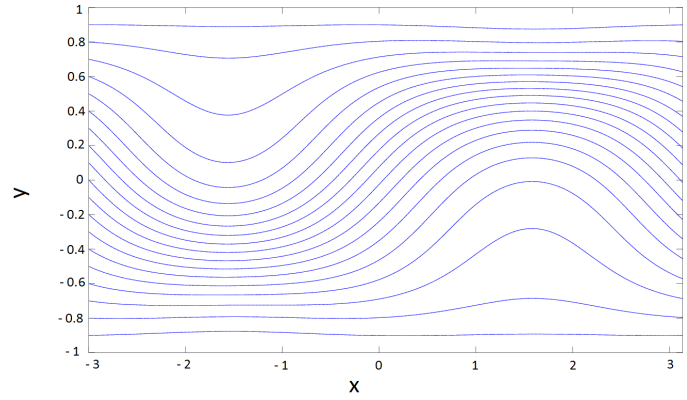

(a)

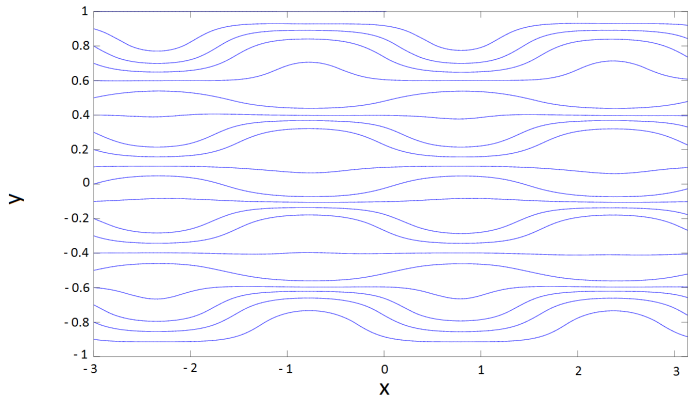

(b)

Figure 5.4: Streamlines of the velocity field for the 2D porosity modulation function. a) kx=1, ky=π b) kx=2, ky=4π.

form, the overall diffusion (equal to total flux because the convection term is null without velocity) decreases a little. It should be remarked that the local porosity value affects the effective diffusion that here has been modeled by the Bruggeman correction see paragraphs 2.2.3 and 3.2.2. Conversely, the flux in the presence of flow is always higher than the corresponding case without flow, however for large ky it could be smaller than the reference case with uniform porosity. For both streamwise porosity modulations, the maximum flux is obtained at the smallest wallnormal wavenumber, i.e. ky=π, being 35%$\div$40% higher than the reference

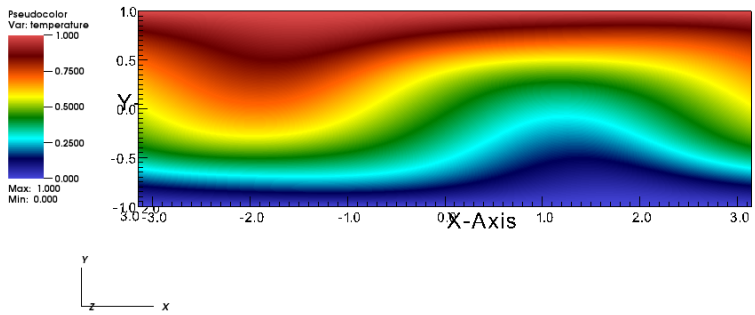

(a)

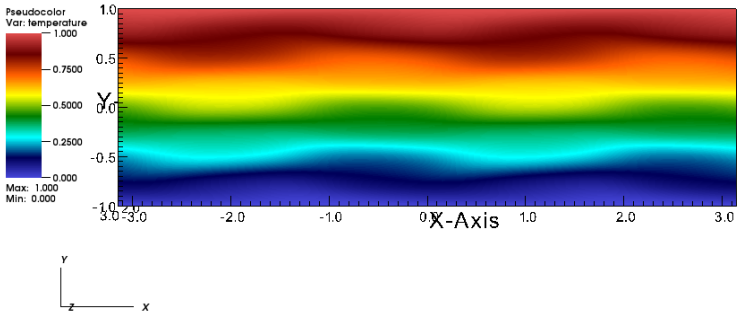

(b)

Figure 5.5: Mass concentration field at steady-state for two different porosity modulations a) kx=1, ky=pi b) kx=2, ky=4pi

case at uniform porosity. Increasing ky the flux always decreases and it is also possible that it becomes lower than the reference case with uniform porosity. In other words the convection always increases the flux, but the modulation of the porosity reduces itself the overall mass transfer changing the local and overall effective diffusion coefficient, i.e. $D_e = \varepsilon^{1.5} D$.

5.2.2 3D simulation

In this subsection we present the results obtained using a tridimensional modulation of the porosity in the media, i.e. using a function which depends on kx, ky and kz. The sequence in which the results are shown is the same as the 2D cases, but every field is now in 3 dimensions. For a better understanding, these are shown by

Porosity constant red is without flow	1 1		
2D kz=0	kx=0.5	kx=1	kx=2
ky=π	1.3911 0.9564	1.3571 0.9662	1.2857 0.9849
ky=2π	1.0802 0.9525	1.1597 0.9551	1.2774 0.9849
ky=4π	0.9753 0.9498	0.9858 0.9504	1.0162 0.9527
ky=6π	0.9573 0.9489	0.9606 0.9484	0.9684 0.9491

Table 5.2: Mass flux at steady state for different wave numbers of the porosity distribution normalized by the value for uniform porosity (F_{cost} = 0.205). In red: simulation results with no flow inside the channel (zero velocity) , in black: with flow (volume flow rate constant).

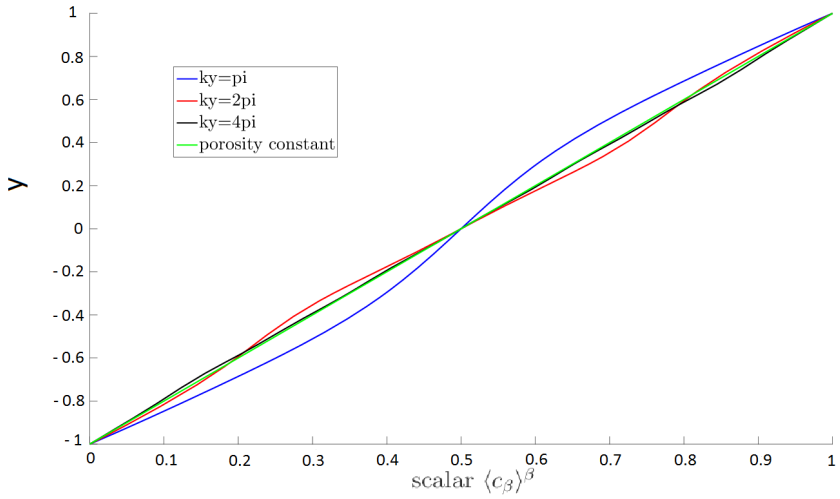

Figure 5.6: Mean value of mass concentration averaged on each streamwise-spanwise plane along wallnormal direction. Results obtained with different ky are compared with result obtained with constant porosity.

different slices of the entire volume and also by isosurfaces.

In the figs. 5.8(a) , 5.8(c) and 5.8(b), 5.8(d) streamwise x-velocity fields are presented. The figs. 5.8(a) , 5.8(c) refers to a field due to a porosity function with frequencies kz=1, kx=1, ky=π and the other two with kz=2, kx=2, kz=4π. As in the 2D case, it is possible to see how the velocity field has the same behavior of the porosity function modulation.

The same evaluations can be made for the other velocity components. Wallnormal y-velocity field is shown in the figs. 5.9(a), 5.9(c), 5.9(b) , 5.9(d) and the spanwise z-velocity field in the figs. 5.10(a), 5.10(c),5.10(b) , 5.10(d), with the same porosity functions as the previous examples. It is important to mark the shape of these fields: in 2D the velocity assumes a cylindrical shape because the porosity is not modulated in spanwise z-direction; in 3D, also the spanwise z-direction is modulated and then the velocity field assumes a spherical shape, with the same

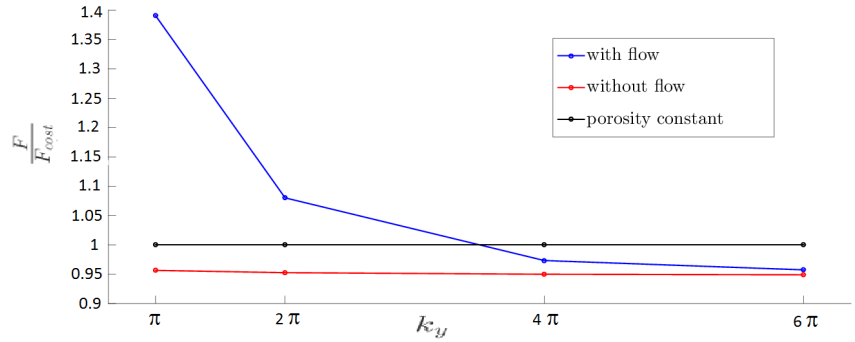

(a)

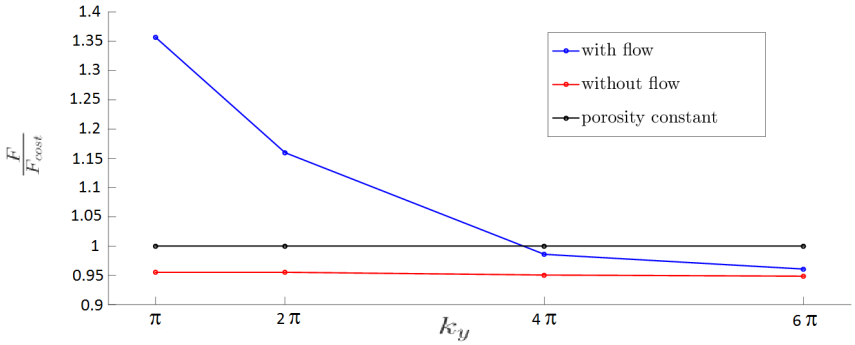

(b)

Figure 5.7: Values of the mass flux with and without flow as a function of ky. (kx and kz fixed) a) kx=0.5, b) kx=1.

frequency of the porosity modulation function.

The mass concentration fields for the same porous functions is shown in the figs. 5.11(a) , 5.11(c), 5.11(b) and 5.11(d). The figs. 5.11(a) and 5.11(c) represent the mass concentration fields with a porosity function with lower frequencies compared to the other two figs 5.11(b) and 5.11(d). As explained in 2D cases (figs. 5.5(a) and 5.5(b)), the porosity function with the lowest frequencies has the highest fluctuation and then the highest flux.

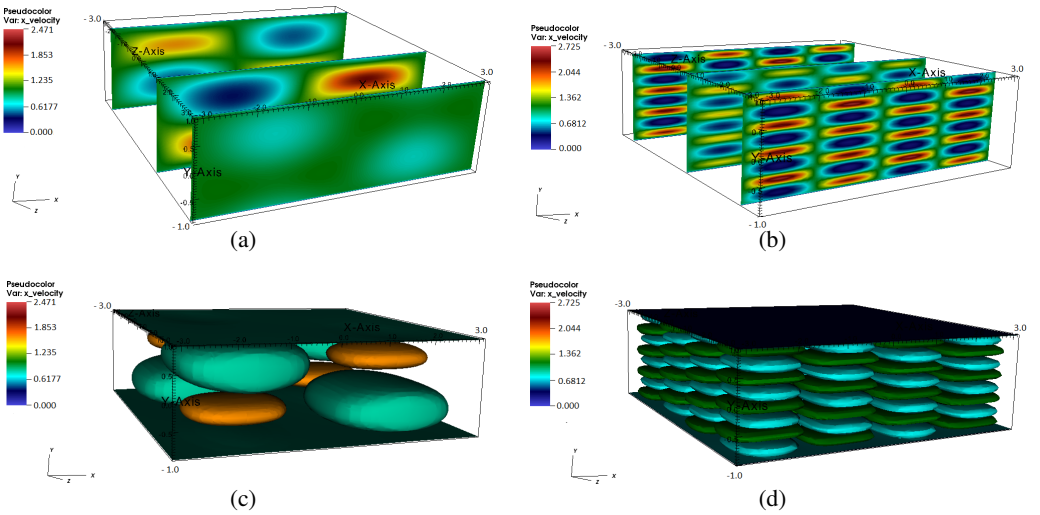

Figure 5.8: Streamwise-velocity due to the porosity function. a) c) slices and isosurfaces with kz=1, kx=1,ky=π. b) d) slices and isosurfaces with kz=2, kx=2, ky=4π.

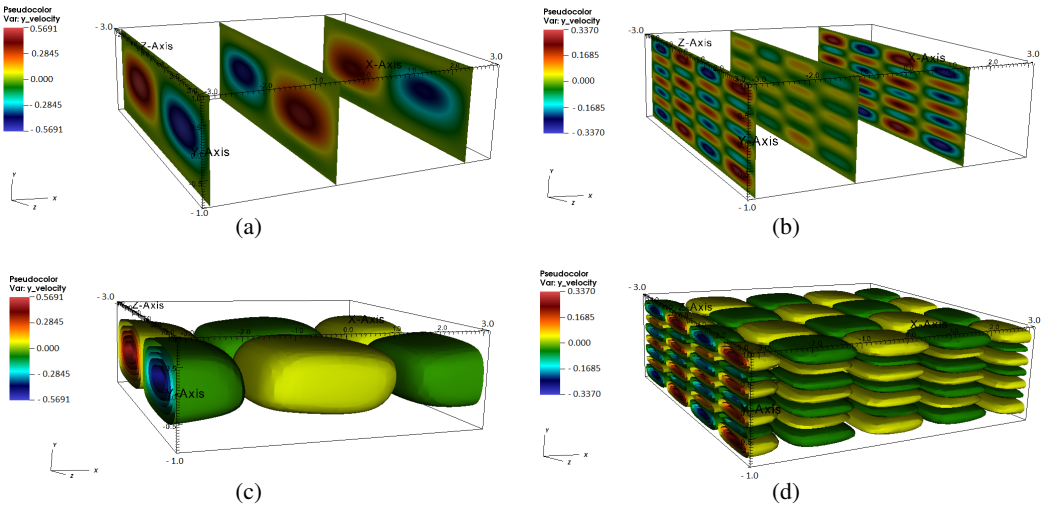

Figure 5.9: Wallnormal-velocity due to the porosity function. a) c) slices and isosurfaces with kz=1, kx=1,ky=π. b) d) slices and isosurfaces with kz=2, kx=2, ky=π.

Also an example of the mean mass concentration value on each x-z plane (perpendicular to wall normal direction) is shown in fig. 5.12. It is clear that, in this case,

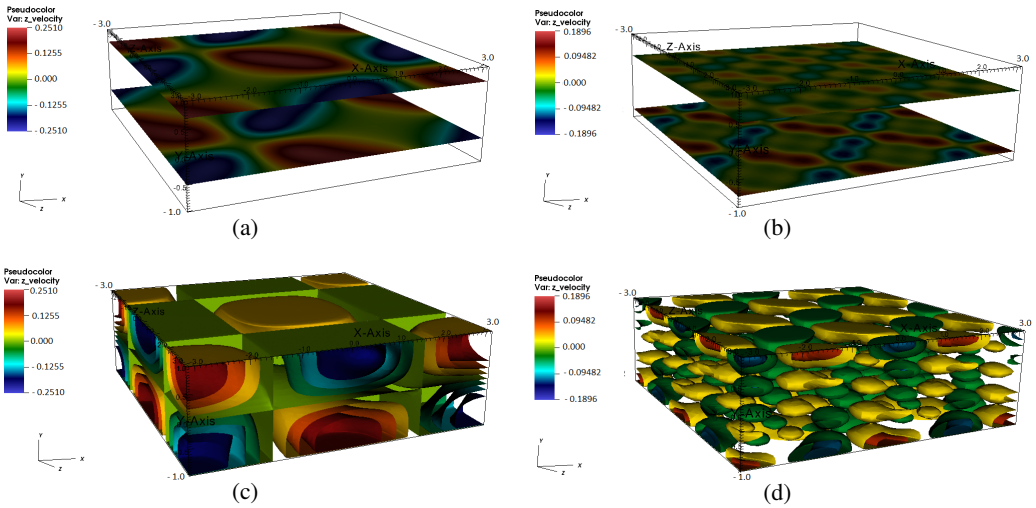

Figure 5.10: Spanwise-velocity due to the porosity function. a) c) slices and isosurfaces with kz=1, kx=1,ky=π. b) d) slices and isosurfaces with kz=2, kx=2, ky=π.

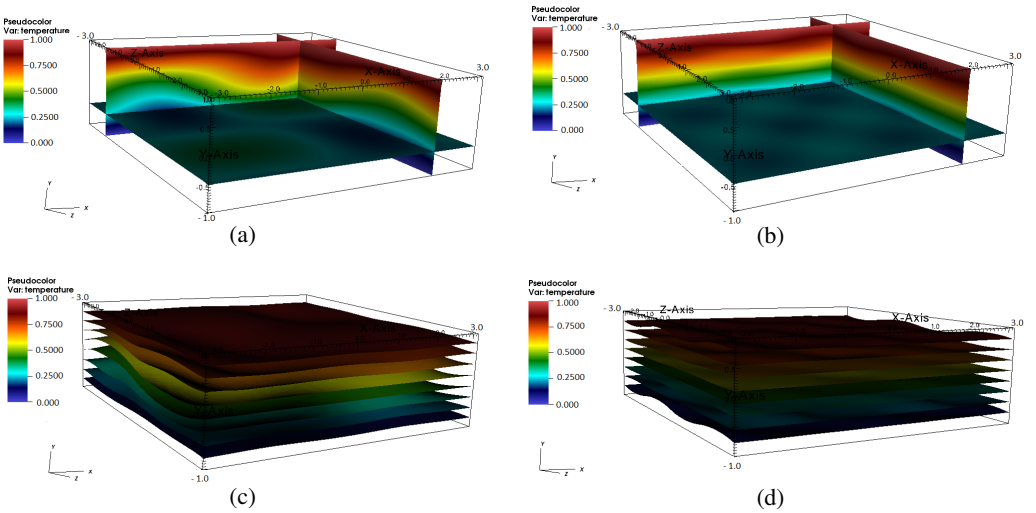

Figure 5.11: Mass concentration fields due to the porosity function. a) c) slices and isosurfaces with kz=1, kx=1, ky=pi. b) d) slices and isosurfaces with kz=2, kx=2, ky=4π.

the difference between the profiles and the reference case are lower compared the 2D case (see fig. 5.6 ky=π - blue line) and these 3D cases will show lower total flux than the 2D cases. It will be shown later that more the profile is different from

the reference case (constant porosity) and higher is the mass flux.

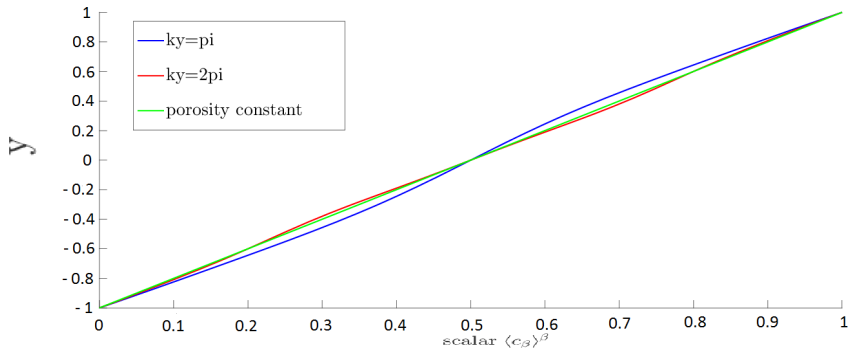

Figure 5.12: Mean value of mass concentration on each streamwise-spanwise plane along wallnormal direction for 3D porosity functions with kz=1 and kx=1 fixed. Results obtained with different ky are compared with result obtained with constant porosity.

Now we will discuss, the overall flux of all the 3D cases that have been reported in tables 5.3 and 5.4. Tab. 5.2 shows results obtained with kz=1 and tab. 5.3 with kx=2.

The last figures shown in this 3D results presentation are the plot of the total mass flux (with and without flow), normalized by the reference case that is the one with uniform porosity, as a function of different frequencies. First we show the results fixing the porosity modulation in the streamwise direction at kx=1. Figure 5.13 shows the total mass flux as a function of ky for increasing frequency of the spanwise porosity modulation, i.e. kz. Generally, we observe a decrease of the effectiveness of the porosity modulation in enhancing the mixing when kz is increased, so the higher mass flux is obtained for kz=0, i.e. 2D geometry. This is a general trend observed also at different streamwise porosity modulation kx.

However, it is interesting to observe the behavior fixing the spanwise porosity modulation kz and changing kx (main plot) or ky (insets), see Figs. 5.14(a) and 5.14(b).

Porosity constant red is without flow	1 1		
3D kz=1	kx=0.5	kx=1	kx=2
ky=π	1.0909 0.9843	1.1608 0.9874	1.1419 0.9940
ky=2π	1.0319 0.9779	1.0802 0.9790	1.1398 0.9823
ky=4π	0.9850 0.9759	0.9928 0.9762	1.0107 0.9772
ky=6π	0.9779 0.9745	0.9801 0.9746	0.9851 0.9751

Table 5.3: Mass flux at steady state for different wave numbers of the porosity distribution normalized by the value for uniform porosity (F_{cost} = 0.205). In red: simulation results with no flow inside the channel (zero velocity) , in black: with flow (volume flow rate constant).

Porosity constant red is without flow	1 1		
3D kz=2	kx=0.5	kx=1	kx=2
ky=π	1.0719 0.9929	1.1040 0.9940	1.1122 0.9972
ky=2π	1.0135 0.9816	1.0570 0.9823	1.1160 0.9847
ky=4π	0.9822 0.9770	0.9898 0.9773	1.0080 0.9781
ky=6π	0.9768 0.9750	0.9791 0.9751	0.9844 0.9755

Table 5.4: Mass flux at steady state for different wave numbers of the porosity distribution normalized by the value for uniform porosity (F_{cost} = 0.205). In red: simulation results with no flow inside the channel (zero velocity) , in black: with flow (volume flow rate constant).

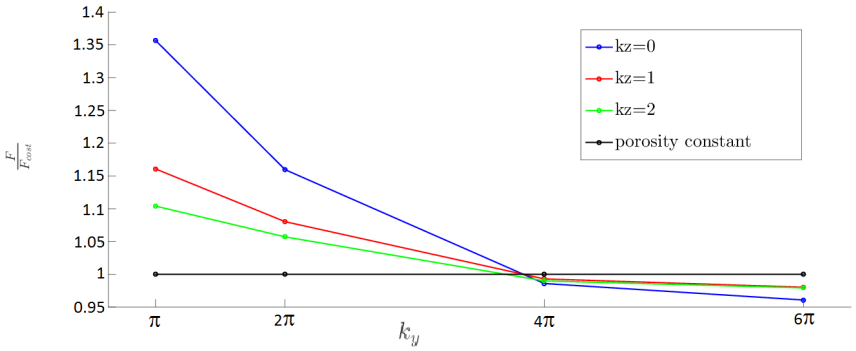

Figure 5.13: Values of the total mass flux as a function of ky for different kz at fixed kx=1

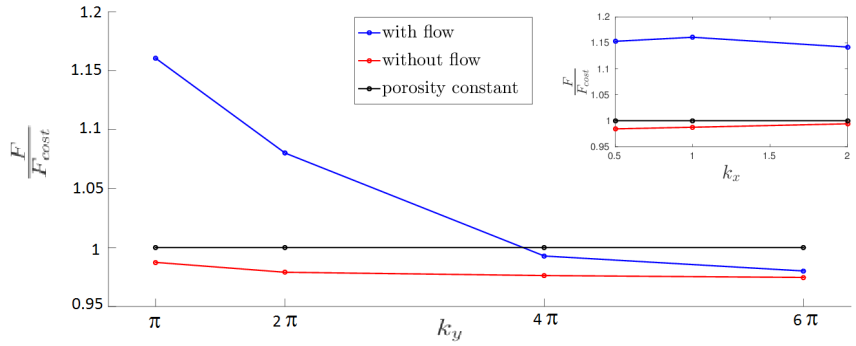

(a)

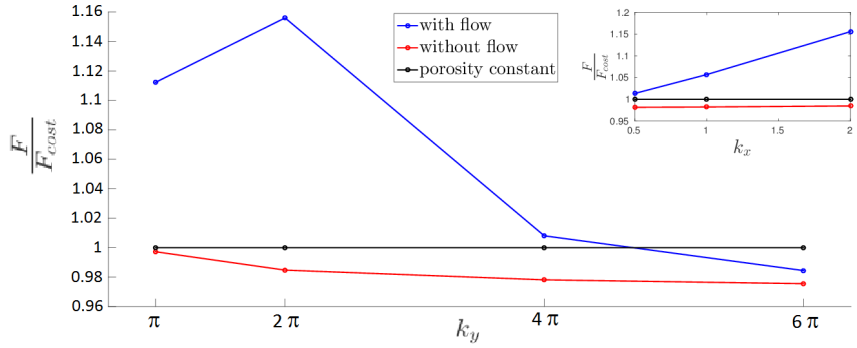

(b)

Figure 5.14: Values of the mass flux with and without flow normalized by the value at constant uniform porosity as a function of ky in the main plots and of kx in the inset. a) kz=1; main plot kx=1 and inset ky=π, b) kz=2; main plot kx=2 and inset ky=2π.

Fixing kz=1 and kx=1 (fig. 5.14(a)), we observe a behavior modulating the porosity in the wallnormal direction ky that is similar to what noted for 2D cases: Higher the wallnormal modulation lower is the total mass flux, which can be below the uniform porosity reference case for large ky as in 2D cases. Fixing kz=1 and ky=π and varying the streamwise modulation of the porosity kx we observe an almost constant flux with a small peak at kx=1. More interestingly, we can note a peculiar behavior in the main plot of figure 5.14(b) where the porosity is modulated fixing kz=1 and kx=2. Actually a well defined maximum appears at ky=2π. In addition looking to the inset, where kz=2 and ky=2π are kept constant, we note an increase of the flux increasing the streamwise modulation. Hence these results show that there is an optimal distribution of the porosity to increase the flux, hence not in all cases lower is the frequency of modulation better is the mixing. In the next section, we propose an interpretation of these results which is able to determine the optimal modulation frequency by comparing the typical diffusion and advection time scales. This theory is able to explain all the behaviors we have discussed.

5.3 Analysis of the results

5.3.1 Effect of the advection on the mass transport

In this section we analyze the variations of the total mass flux observed when the porosity modulation is operated.

First we show the relative importance of the diffusion and convection term which compose the total mass flux; recalling the eq. (3.22) the total flux is given by:

$$\nabla \cdot (\varepsilon_\beta \langle \mathbf{v}_\beta \rangle^\beta \langle c_\beta \rangle^\beta - \varepsilon_\beta \mathbf{D}_e \cdot \nabla \langle c_\beta \rangle^\beta) = 0$$

where we recognize

- the convective term: $\varepsilon_\beta \langle \mathbf{v}_\beta \rangle^\beta \langle c_\beta \rangle^\beta$

- the diffusive term $\varepsilon \mathbf{D}_e \cdot \nabla \langle c_\beta \rangle^\beta$.

To analyze data it is necessary to introduce an average on the homogeneous directions x and z: $\overline{c} = (1/A_{x,z}) \int_{x,z} c dx dz$ with c a generic quantity. Hereafter we consider an isotropic medium so the diffusivity becomes a scalar and we skip brackets and subscripts. Averaging eq.(3.22) and considering the homogeneity of present channel we obtain,

$$\frac{d}{dy}\left(\overline{\varepsilon v_y c} - \overline{\varepsilon D_e \frac{dc}{dy}}\right) = 0 \tag{5.1}$$

and

$$\overline{\varepsilon v_y c} - \overline{\varepsilon D_e \frac{dc}{dy}} = F_{tot} \tag{5.2}$$

with F the average mass flux that is constant through the channel height. Clearly if the medium is uniform and the flow parallel the mean concentration is linear because the average quantities coincide with the local, $v_y = 0$ and D_e is constant. If there is no flow, but the porosity is modulated in the space the convective term is null. However we remark that the mean concentration is not linear since it is constant $F_d = -\overline{\varepsilon D_e \frac{dc}{dy}} = F_{tot}$ because D_e spatially varies.
How the advective $F_a = \overline{\varepsilon v_y c}$ and diffusion $F_d = -\overline{\varepsilon D_e \frac{dc}{dy}}$ terms compose the total mass flux F_{tot} is shown in figs. 5.15, 5.16 and 5.17. Each color line represents the value of the diffusive term normalized by the total flux F_d/F_{tot} along the wall normal direction. At the walls the convective term is null and the diffusive term equals the total flux and thus, so $F_d/F_{tot} = 1$. Using this normalization it is possible to assess the effect of the convective and diffusive terms composing the total flux. The sketched area between the color curves and the black line is equivalent to the contribution of convective flux, instead the white area between the color curves and the y axis is the diffusive flux.

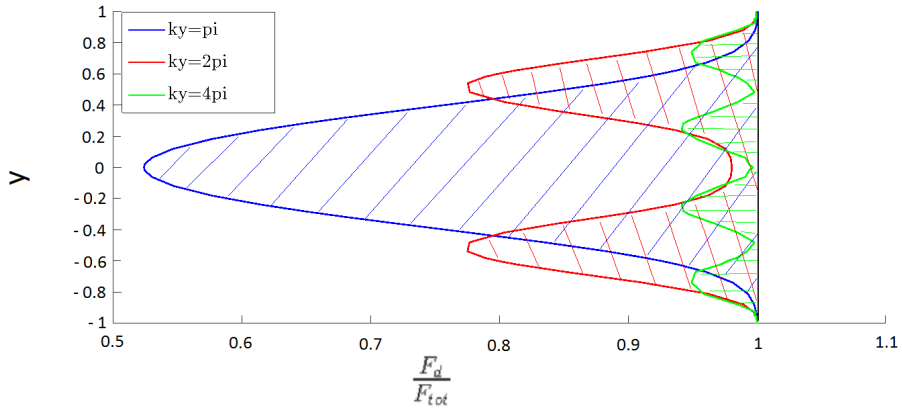

Figure 5.15: Ratio between the diffusive flux and the total flux F_d/F_{tot} as a function of the porosity modulation in ky, fixing kz=0 and kx=0.5. The sketched area represents the overall contribution of the convective flux.

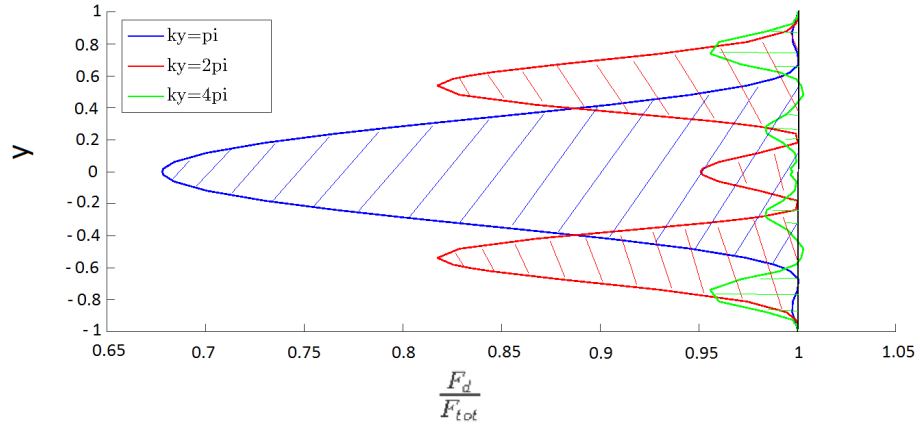

Figure 5.16: Ratio between the diffusive flux and the total flux F_d/F_{tot} as a function of the porosity modulation in ky, with kz=1 and kx=1. The sketched area represents the overall contribution of the convective flux.

The first observation, looking at these images, is that the number of peaks of each curve is equal to the number of the period of the porosity function, due to the different ky. Hence the number of the peaks is also equal to the number of the oscillations of velocity and scalar fields. Moreover, the zones, along the wall normal direction, where the convective flux is higher (corresponding to the peaks) coincide to the zone where the scalar undulations occur, see e.g. figs. 5.5(a) and

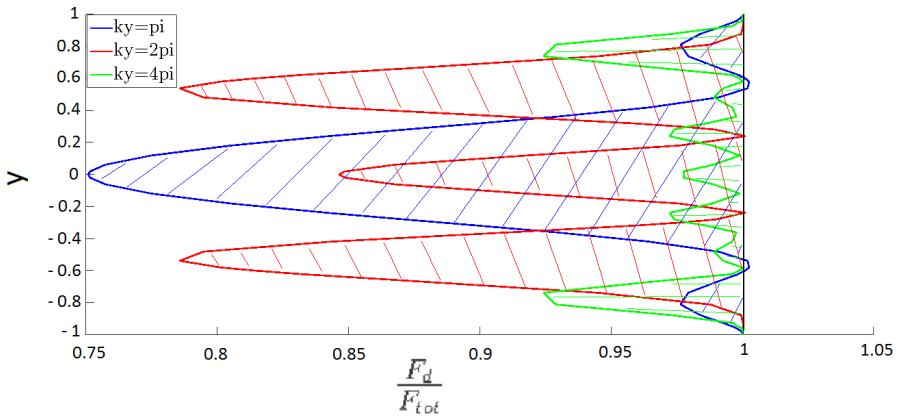

Figure 5.17: Ratio between the diffusive flux and the total flux F_d/F_{tot} as a function of the porosity modulation in ky, with kz=2 and kx=2. The sketched area represents the overall contribution of the convective flux.

5.5(b).

Increasing the frequency in the spanwise direction more peaks appear and the difference between peaks decreases.

Looking at the values of the convection terms, it is possible to note that when the wavenumber in spanwise and wall normal direction (kz and ky) are increased, the rate of the convective flux decreases. This means that the convective term has the same trend as the total mass flux and, in fact, the cases where the convective term is higher also the total flux is higher (compare fig. 5.15, 5.16, 5.17 with tab. 5.2,5.3 and 5.4).

Hence appears that promoting large scale motion across the channel increases the advective terms and in turns the overall mass fluxes. In other words high frequency porosity modulations are not able to excite these long-range motions and are less effective to promote advective mass transfer. To better clarify this behavior, we show that generally higher the mass flux higher the wall-normal velocity intensity is, see fig. 5.18 for a 2D porous medium with kx=0.5. Since large scale porosity modulation are usually associated to higher wall-normal velocity we note that

modulation of the porosity at low wave numbers is more effective to enhance mixing. However this property is not always true. As can be appreciated in fig. 5.19

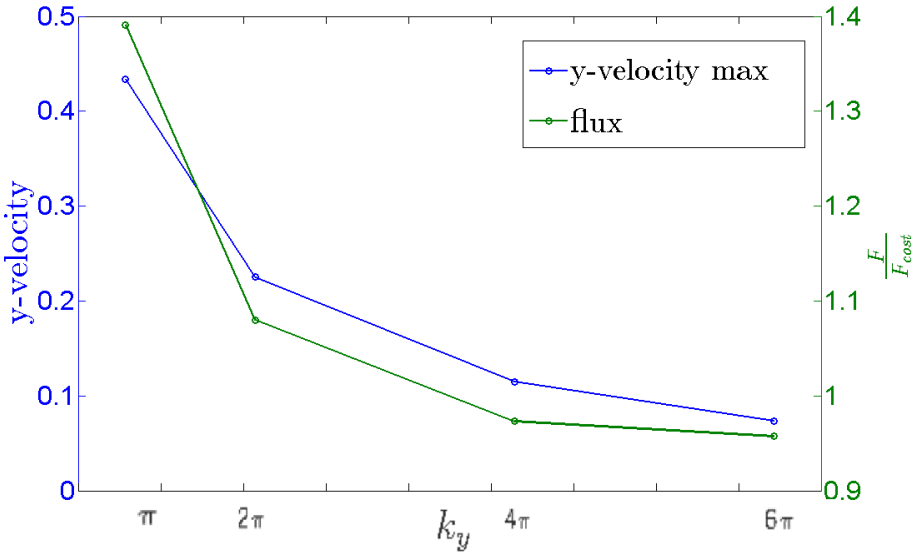

Figure 5.18: Plot of the maximum value of the wallnormal-velocity in the field and the normalized mass flux vs ky. The porosity distribution is characterized by kz=0 and kx=0.5

for a porous medium with kx=kz=2, the mass flux does not exactly correlate with the intensity of the wall-normal velocity. This behavior suggests that the real interpretation of the results cannot understood only in terms of intensity of convective motions. Actually in the near wall region, where the scalar value is imposed, the velocity is small hence diffusive dynamics leads the process.

This aspect calls for a comparison of the typical time scale of the two phenomena in order to determine the optimal modulation of the porosity to increase the mixing.

5.3.2 Interpretation of the results with characteristic time-scales

The modulation of the porosity seems to be more effective at low wavenumbers. However, while in the wall-normal direction we are constrained with a lower bound

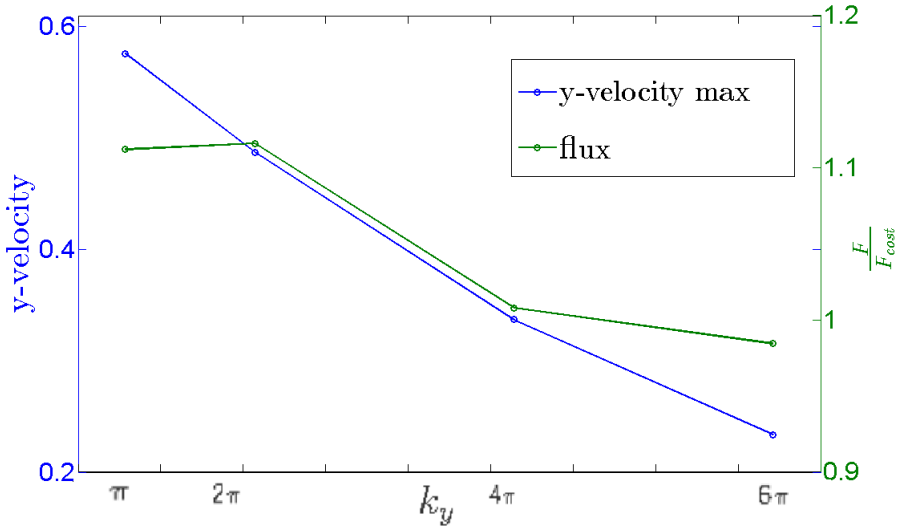

Figure 5.19: Plot of the maximum value of the wallnormal-velocity in the field and the normalized mass flux vs ky. The porosity distribution is characterized by kz=2 and kx=2

due to the channel thickness, i.e. $kx_{min}=\pi$, this is not the case for the streamwise direction where we can consider frequency as low as desired. Nonetheless if we consider a modulation of the porosity with $kx \rightarrow 0$ the streamlines assume an horizontal shape without any curvature and in this case the total mass flux is the minimum, see tab. 5.2. This means that fixing ky and kz, an optimal function for assign the porosity exists with finite kx. In fig. 5.20(a) we show the normalized mass flux for porous media characterized by kz=0, different ky and as a function of kx. The mass flux for ky=π shows a maximum for kx$\simeq$ 0.5, while the maximum for higher ky appears for kx higher than that simulated in the present work. A similar behavior is shown in fig. 5.20(b) for kz=1 where for ky=π the maximum appears at kx$\simeq$ 1 and at higher kx for higher ky.

Here, we propose a phenomenological interpretation which can able to explain the order of magnitude of the porosity modulation wavenumbers kx,ky,kz to maximize the mass flux. The theory is based on dimensional analysis of the typical time

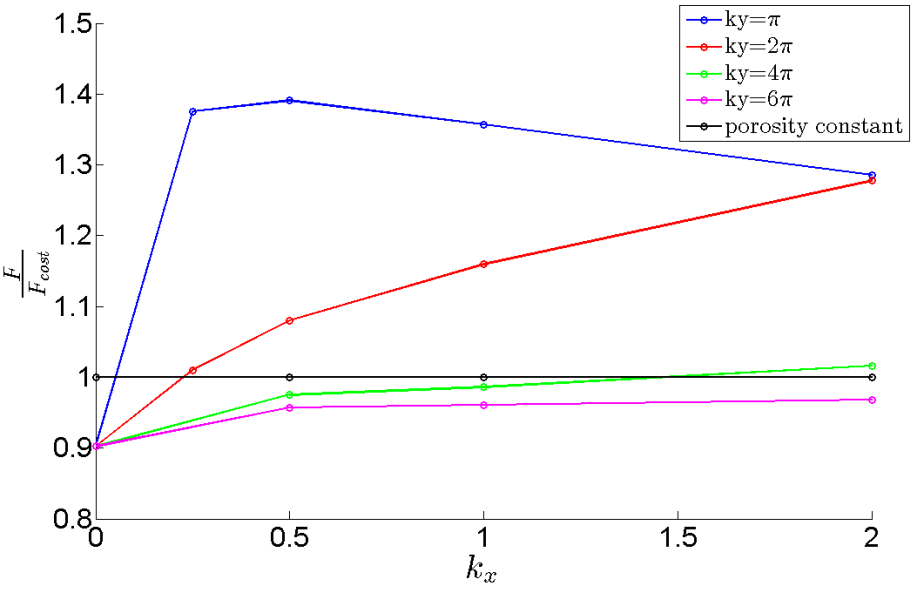

(a)

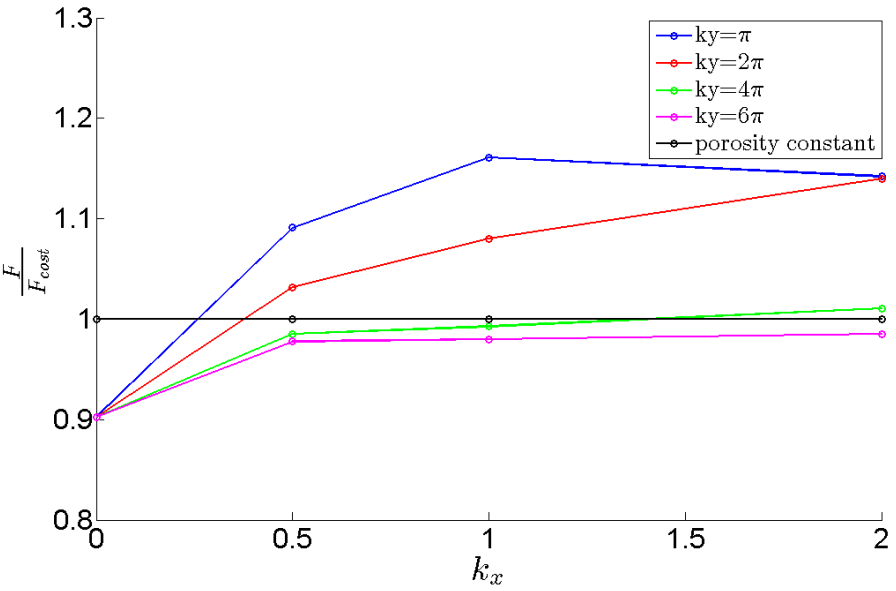

(b)

Figure 5.20: Total mass flux normalized by the uniform porosity case for different porosity modulation as a function of kx for different ky with kz fixed. a) kz=0 b) kz=1.

scales and is by definition approximate. We first refer to the case with ky=π where only one oscillating stream of scalar exists through the walls. The basic assumption is that the convective stream between the walls should occur in "enough time" so it can be enriched by the scalar via diffusive processes. Figure 5.21 provides

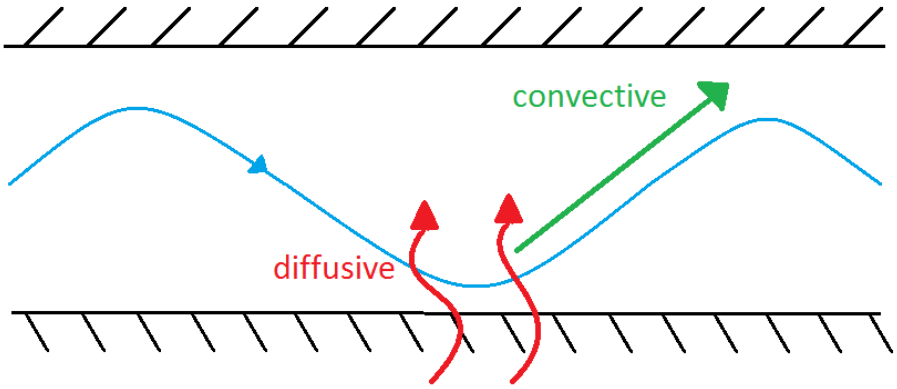

Figure 5.21: Sketch of the transport process occurring in the porous media when a single oscillation in the wall normal direction is considered.

a graphical sketch of the model. In other words, the typical time scale of the diffusion should match the typical time scale of advection in order to enhance the mass transport across the wall. If one of the two phenomena become much faster the other slow down the process. To assess the validity of this statement we need to calculate the typical time scales of these processes for the optimal cases previously highlighted and check that they have the same order of magnitude. The characteristic diffusion time is defined as:

$$t_D = \frac{L_T^2}{D} \tag{5.3}$$

where D is the diffusion coefficient and L_T is the typical transversal length where diffusion occurs. It can be estimated as the half of the wavelength in the transversal wall-normal direction (the distance from the wall to the half of the oscillation of

the stream):

$$L_T = \lambda_y/2 = \pi/ky. \tag{5.4}$$

The characteristic convective time (fixing ky=*pi*) is defined as:

$$t'_C = \frac{L_S}{u} \tag{5.5}$$

where u is the typical advection velocity that can be estimated by the bulk velocity u_b and L_S is the advection characteristic length, estimated by half wavelength of the stream oscillation:

$$L_S = \lambda_x/2 = \pi/kx. \tag{5.6}$$

Hence we can define the ratio of the characteristic time scales R'_t as

$$R'_t = \frac{t_D}{t'_C} = \frac{\pi^2/(D\,ky^2)}{\pi/(u_b\,kx)} = \frac{\pi u_b\,kx}{D\,ky^2}, \tag{5.7}$$

which should be order one to produce an optimal mass transfer: $R_t = O(1)$.

Calculating R_t [1] using the simulation parameters for the maximum shown in figure 5.20(a), i.e. kx=0.5 ky=π kz=0, we obtain $R'_t \simeq 1.5$. Actually, assuming $R'_t = 1$ and estimating the optimal kx, we obtain $kx = \pi/10 \simeq 0.31$ which is very close to the location of the optimal transfer. Hence for the maximum shown for $ky = \pi$ the typical convective and diffusive time scales are of the same order of magnitude.

In case we have more oscillating streams in the channel thickness, i.e. $ky \geq 2\pi$, it necessary to expand the proposed model. We will refer to the sketch shown in figure 5.22. The typical diffusive process will occur following the same time scale proposed in eq.(5.3) since the traversal length of diffusion will be the half y-wavelength of the oscillation. However, after a single streamwise oscillation the

[1] in dimensionless units, normalized by h/u_b with h the channel half-width and u_b the bulk velocity, D=0.1

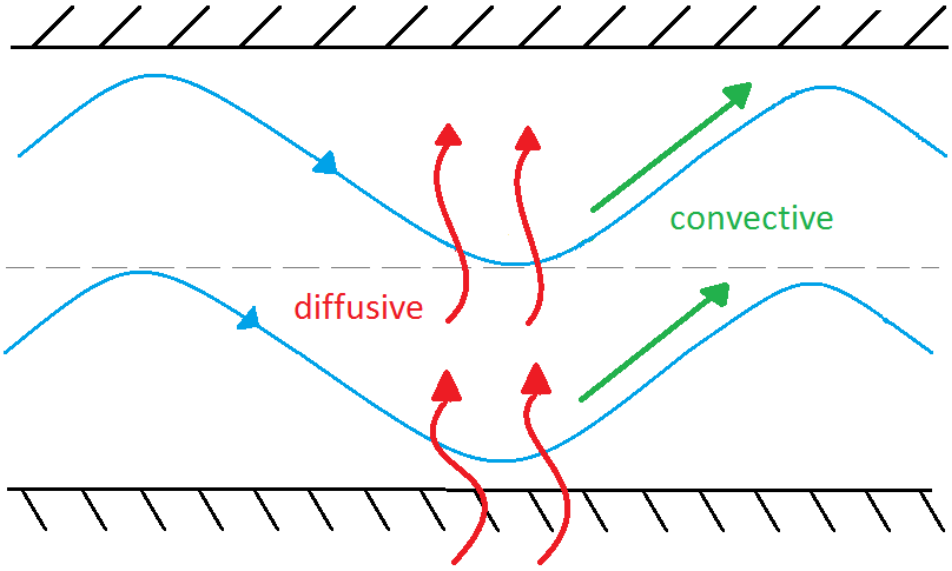

Figure 5.22: Sketch of the transport process occurring in the porous media when more oscillations in the wall normal direction are considered.

scalar concentration diffused from one wall will not arrive to the other wall, but to the next wallnormal oscillating stream, see figure 5.22. At this stage the process needs to be repeated. The total repetitions will coincide with the number of the oscillating streams present in the wall normal direction: $n_s = \pi/ky$. Hence the convective time-scale should be corrected using this factor:

$$t_C = \frac{n_s L_S}{u}. \tag{5.8}$$

The last definition is consistent with the definition of the convective time scale proposed for $ky = \pi$ where $n_s = 1$. When we have more oscillating streams, eq.5.8 implies an effective longer distance to be convectively traveled by the scalars. Hence the final definition for the time scale ratio is:

$$R_t = \frac{t_D}{t_C} = \frac{\pi^2/(D\,ky^2)}{n_s\,\pi/(u_b\,kx)} = \frac{\pi^2 u_b\,kx}{D\,ky^3}, \tag{5.9}$$

which coincides with previous definition of R_t' when ky=π. E.g. focusing on $ky = 2\pi$ we obtain $R_t = 1$ when ky=$8\pi/10 \simeq 2.5$. Looking to the red line in figure 5.20(a) we infer that the maximum will be for kx> 2. Hence it seems that the proposed formula is able to capture the order of magnitude of the optimal porosity modulation in the streamwise direction, kx, when fixed the modulation in the wallnormal direction, i.e. ky. Since R_t does not depend on kz, while the present model may work in 2D, i.e. kz=0, it cannot be strictly used in 3D. Comparing figures5.20(a) and 5.20(b) we observe that the optimal kx wavenumber increases with kz and this is not captured by eq.(5.9). We interpret this result because the characteristic length convectively traveled by the scalar is increased because of the 3D velocity field. It should be remarked that also the diffusion dynamics will be a 3D phenomena and so differences are expected also for this quantity. At the present moment we are not able to extend quantitatively the model for 3D cases, nonetheless it should be noted that the maximum enhancement in the mass transport is obtained in 2D cases. Hence from a practical perspective, using simple harmonic function it is more convening to use 2D porosity modulations that appears well described by the proposed simple model.

Chapter 6

Alternative method to evaluate mixing: scalar variance

In this chapter, we present data on the mixing enhancement not for a steady-state case but in transient condition. The idea is to evaluate the mixing inside the channel by looking at the time needed to homogenize a mixture. We will analyze the time evolution of the scalar variance. The first section is dedicated to explain the physical case and its setup. Then the equation to describe the scalar variance of a fluid flows through a porous media will be presented. The last part discusses the results obtained using two different types of initial conditions.

6.1 Simulation set-up

In these simulations, we changed only the boundary and initial conditions with respect to the cases presented in section 5.1.

For the boundary conditions, insulated walls are imposed to the upper and lower surfaces $\mathbf{v} = 0$, $\frac{\partial c}{\partial y} = 0$. This means that the mass concentration values are not fixed but the mass transfer flux through the surfaces is null.

The initial conditions for the scalar value are not linear along the wall normal direction, but the channel is divided in two or more slots, where the mass concentration assumes a constant value. We run the simulations with only two types of initial conditions; in the first, the channel is split in half: the upper volume has mass concentration equal to +1 and lower equal to -1. In the second set up, the channel is divide in three parts and the values are +1 on the zones near the wall and -1 in the middle zone of the channel. A linear variation is imposed on the interface zones that however have a small thickness. (see fig. 6.1 and 6.2).

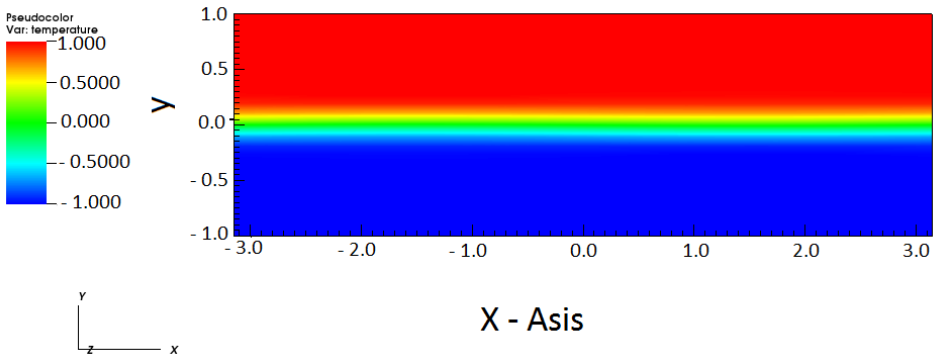

Figure 6.1: Initial condition for the mass transfer concentration. Channel is initially divided in two zones of different concentration.

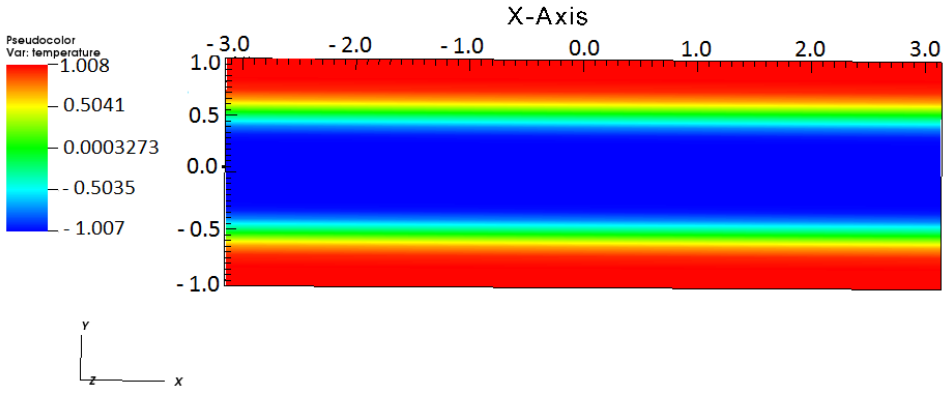

Figure 6.2: Initial condition for the mass transfer concentration. The channel is initially divided in three zones of different concentration.

6.2 Scalar variance function

To evaluate how fast is the mixing we need to introduce a function that measures the inhomogeneity of the scalar concentration field. We will assume that the concentration field is with null mean value (fluctuations). The scalar variance averaged in the volume is defined as,

$$\Theta = (1/V) \iiint \varepsilon \left(\frac{c^2}{2}\right) dV$$

, where a vanishing value indicates a fully mixed field. We can connect this quantity with the concentration field evolution that is described in the following. From the mass transfer equation (eq. 3.20) we try to obtain a new formulation which describes the mass variance. To make the notiation simpler as in chapter 3, we do not write every term as a function of β. Eq. (3.20) can be rewritten as :

$$\frac{\partial c}{\partial t} + \nabla \cdot (\varepsilon c \mathbf{v}) = \nabla(\varepsilon D_e) \cdot \nabla c + \varepsilon D_e \nabla^2 c \tag{6.1}$$

Using the indicial notation and expanding the divergence, this equation becomes:

$$\varepsilon \frac{\partial c}{\partial t} + \varepsilon \mathbf{v}_j \frac{\partial c}{\partial x_j} + c \frac{\partial (\varepsilon \mathbf{v}_j)}{\partial x_j} = \frac{\varepsilon D_e}{\partial x_j} \frac{\partial c}{\partial x_j} + \varepsilon D_e \frac{\partial^2 c}{\partial x_j \partial x_j} \tag{6.2}$$

The third term on the left hand side is the continuity equation and from eq. 3.9 is null. Each term, now, is multiplied by the scalar value c:

$$\varepsilon \frac{\partial}{\partial t}\left(\frac{c^2}{2}\right) + \varepsilon \mathbf{v}_j \frac{\partial}{\partial x_j}\left(\frac{c^2}{2}\right) = \frac{\varepsilon D_e}{\partial x_j} \frac{\partial}{\partial x_j}\left(\frac{c^2}{2}\right) + c\varepsilon D_e \frac{\partial^2 c}{\partial x_j \partial x_j} \tag{6.3}$$

Rewriting the second term on the right hand side:

$$\varepsilon \frac{\partial}{\partial t}\left(\frac{c^2}{2}\right) + \varepsilon \mathbf{v}_j \frac{\partial}{\partial x_j}\left(\frac{c^2}{2}\right) = \frac{\varepsilon D_e}{\partial x_j} \frac{\partial}{\partial x_j}\left(\frac{c^2}{2}\right) + \varepsilon D_e \frac{\partial}{\partial x_j}\left(c \frac{\partial c}{\partial x_j}\right) - \varepsilon D_e \left(\frac{\partial c}{\partial x_j} \frac{\partial c}{\partial x_j}\right) \tag{6.4}$$

and again:

$$\varepsilon\frac{\partial}{\partial t}\left(\frac{c^2}{2}\right)+\varepsilon\mathbf{v}_j\frac{\partial}{\partial x_j}\left(\frac{c^2}{2}\right)=\frac{\varepsilon D_e}{\partial x_j}\frac{\partial c}{\partial x_j}+\frac{\partial}{\partial x_j}\left(\varepsilon D_e c\frac{\partial c}{\partial x_j}\right)-\frac{\varepsilon D_e}{\partial x_j}\frac{\partial c}{\partial x_j}-\varepsilon D_e(\nabla c)^2 \quad (6.5)$$

If we integrate in the volume the second term on the left hand side is zero because of periodic boundary conditions. Simplifying and integrating, we obtain:

$$\iiint\varepsilon\frac{\partial}{\partial t}\left(\frac{c^2}{2}\right)dV=\iiint\frac{\partial}{\partial x_j}\left(\varepsilon D_e c\frac{\partial c}{\partial x_j}\right)dV-\iiint\varepsilon D_e(\nabla c)^2dV \quad (6.6)$$

The term on the left hand side $\frac{\partial}{\partial t}\iiint\varepsilon\left(\frac{c^2}{2}\right)dV=\frac{\partial}{\partial t}\Theta\,V$ represents the evolution of the variance of the scalar concentration and can be shown to decrease monotonically in time as a closed system.

$$\frac{\partial}{\partial t}\Theta=\frac{1}{V}\iiint\frac{\partial}{\partial x_j}\left(\varepsilon D_e c\frac{\partial c}{\partial x_j}\right)dV-\frac{1}{V}\iiint\varepsilon D_e(\nabla c)^2dV \quad (6.7)$$

The first term on the right hand side is always equal to zero in the present case and then Θ variation in time is due to the second term on the right hand side which is actually a scalar variance dissipation being proportional to a diffusion coefficient and the square of the scalar gradient.. When Θ decreases the mass concentration inside the channel is becoming uniform. The porous function that takes a lower time to decrease Θ can be said to have the higher mixing.

6.3 Results

We analyze the Θ function and its behavior varying the porosity modulation.
As usual, the results are shown as a function of one wavelenght of the porosity function and the other two are fixed. The constant porosity is our reference case.

6.3.1 First type of initial condition

We start our presentation showing the results obtained with the initial condition shown is fig. 6.1. For the 2D simulations, the fig. 6.3(a) refers to the variation of the Θ-function in time and the fig. 6.3(b) refers to the variation in time of the time derivative of the Θ-function (mass transfer variance). When the derivative of the Θ is large, the mixing is faster and thus, Θ-function uses a lower time to arrive to the homogenous condition (equal to zero in all the volume). Fig. 6.3(a) show that mixing decrease when the frequency in wall normal direction (ky) is increased, as already obtained evaluating the mass transfer flux. Also analyzing the same function without any flow thorough the porous media, we obtained the same results as the mass transfer flux, as shown in 6.4(a) and 6.4(b): all the functions, without flow, have less mixing than the reference case (constant porosity) and their mixing is approximately the same. The last images 6.5(a) and 6.5(b) shows for the 2D case the comparison of the same function between flow and without flow through the channel.

These results have the same trend of the other simulations done for the 2D case and then all the plots are not shown.

Also for the 3D case, the trend for the wall normal frequency is the same: when ky is increased mixing decreases. In the fig. 6.6(a) and 6.6(b), instead, the results as a function of kz (frequency on spanwise directions) are shown. Also in this case, when the frequencies of the porosity function are increased we obtain a lower mixing.

With this new analysis and with this initial condition we have obtained the same results of the chapter 4. The higher mixing is obtained with flow through the channel and lower frequencies of the porosity function.

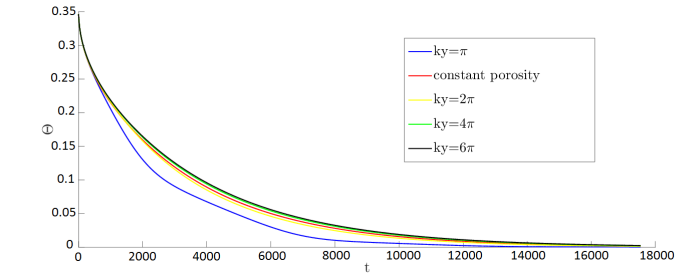

(a)

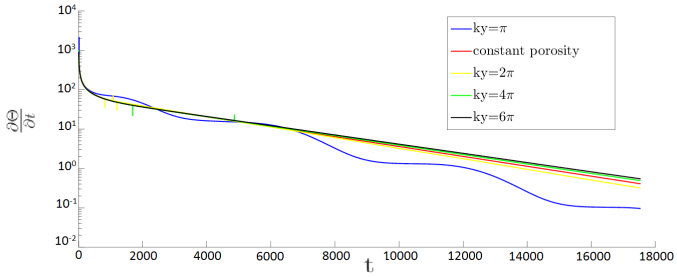

(b)

Figure 6.3: Logarithmic scale in y-axis. a) Θ b) Time derivative of Θ. All the quantities are normalized by h and u_b. The profiles refer to different porosity modulations changing ky, while kz=0, kx=1 are fixed.

6.3.2 Second type of initial condition

The same simulations are repeated but with different initial conditions: fig. 6.2.

From the previous examples, we have understood that the behavior of the variance is the same of the Θ-function; for this reason in this section only the graphics of the mass concentration variance will be shown.

In fig. 6.7 the trend of the variance as a function of ky (kz=0 and kx=2 are fixed) is shown. If this result is compared with the other obtained in this study, it is possible to note that the function with ky=2π is more closer, with these initial conditions, to the function with ky=π. Moreover, in the fig. 6.8, which shown an example in 3 dimensional (kz=1, kx=2), the function with ky=2π has a better mixing than the ky=π function. This result is totally different compared to the results obtained with the first type of initial conditions and also with mass transfer flux simulations.

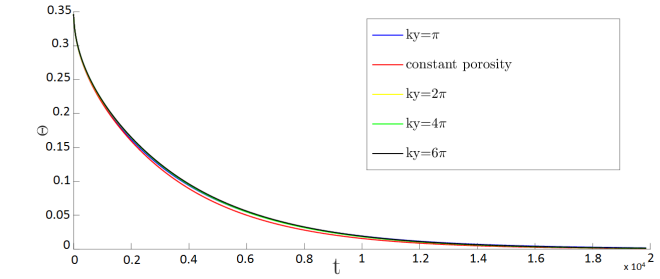

(a)

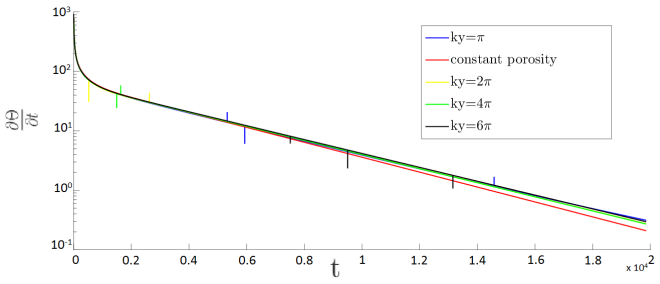

(b)

Figure 6.4: a) Θ vs t b) Time derivative of Θ vs t for cases without flow. The profiles refer to different porosity modulations changing ky, while kz=0, kx=1 are fixed.

Other similar results are obtained with these types of initial conditions.

6.4 Interpretation

The results obtained with this transient-state cases highlight that the choice of the porosity function to optimize the mixing is not univocal. For the initial conditions where the mass concentration inside the channel is divided in two zones, the type of mixing required is similar to the mass transfer from the lower to the upper surfaces, because mixing and mass transportation is necessary in all the volume. Instead, for second type of initial conditions (channel dived in three zones) a global mixing in all the channel is not required. In fact, if we imagine to divide the channel in half, transfer mass from lower to upper wall is not necessary but only mixing into the

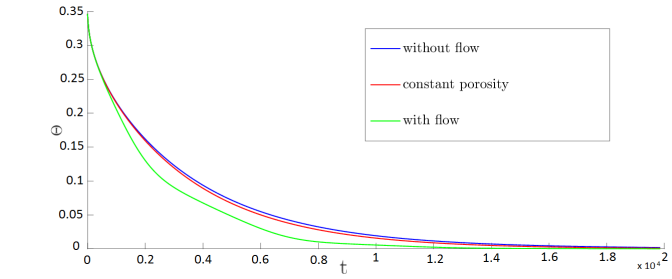

(a)

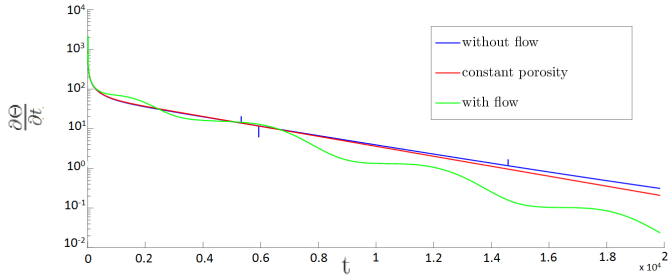

(b)

Figure 6.5: a) Θ b) Time derivative of Θ. Comparison with and without flow. kz=0, kx=1, ky=π.

lower half and the upper half separately (see fig. 6.2). The following figures show what we have just explained: fig. 6.9 shows how the scalar mass concentration field evolve during the time; in this example, porosity function has ky=2π and it is possible to see that this porosity distribution does not work well with this type of initial condition because it can not transport fluid from lower to upper volume. Instead, if the initial conditions are changed, as in figs. 6.10 and 6.11, we can see that both functions work well. In fact, in fig. 6.10 the ky=π-function acts in all the volume fluid moving the mass from bottom to top and vice versa. The fig. 6.11 shows how the ky=2π-function acts on two distinct regions separately and thus, even if it does not transfer fluid from bottom to top, it has an important effect in the two halves, where mixing occurs.

To conclude we can say that modulation with the wider wavelength in the wall-normal directions are optimal for all the transient cases analyzed, even though not

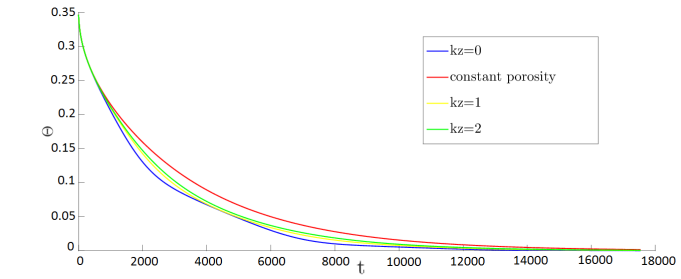

(a)

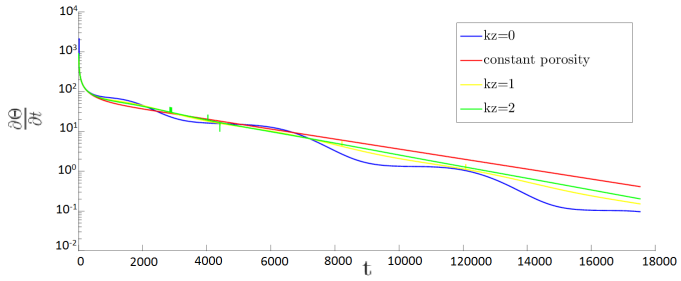

(b)

Figure 6.6: a) Θ b) Time derivative of Θ. Comparison with different kz. kx=1, ky=π are fixed.

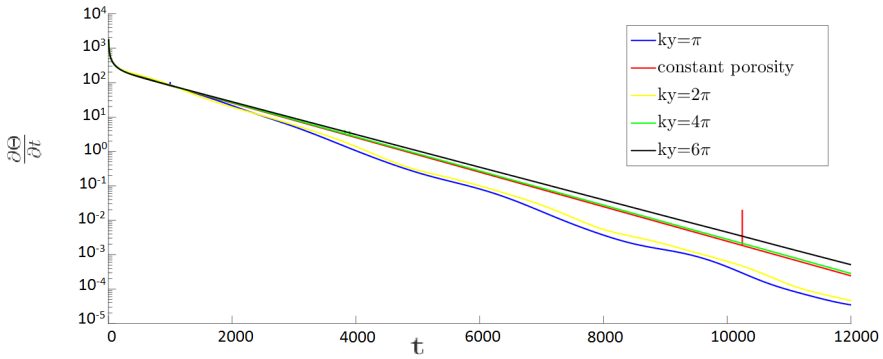

Figure 6.7: Time derivative of Θ obtained with second type of initial conditions. Comparison with different ky. kz=0, kx=2 are fixed.

univocal. In these cases the effect of the modulation in other directions is less important compared to the steady-state analysis. In other words, some porosity modulations that do not increase the mass transfer in the steady-state conditions here work properly, but all the modulations, which are optimal in the steady-state,

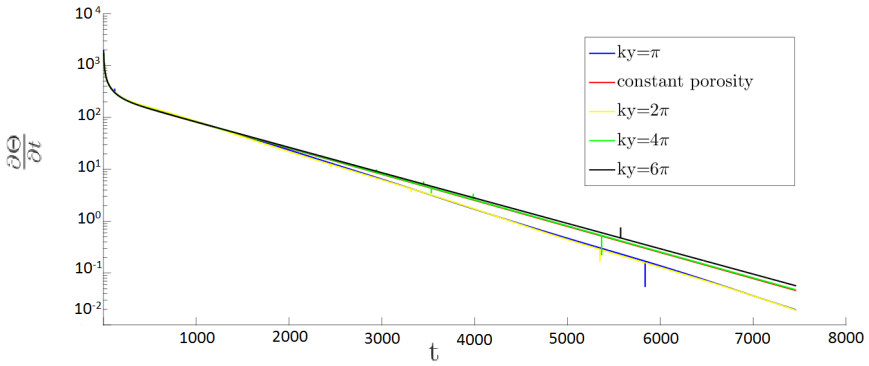

Figure 6.8: Time derivative of Θ obtained with second type of initial conditions. Comparison with different ky. kz=1, kx=2 are fixed.

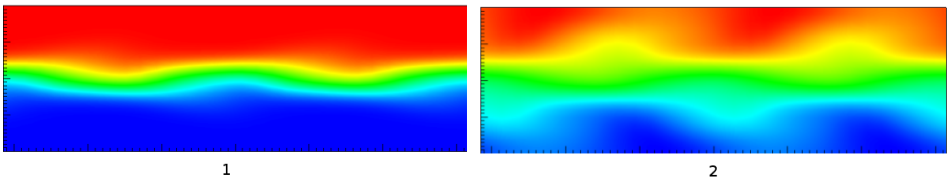

Figure 6.9: Snapshot at different time of mixing with first type of initial condition. Kz=0, kx=2, ky=2pi.

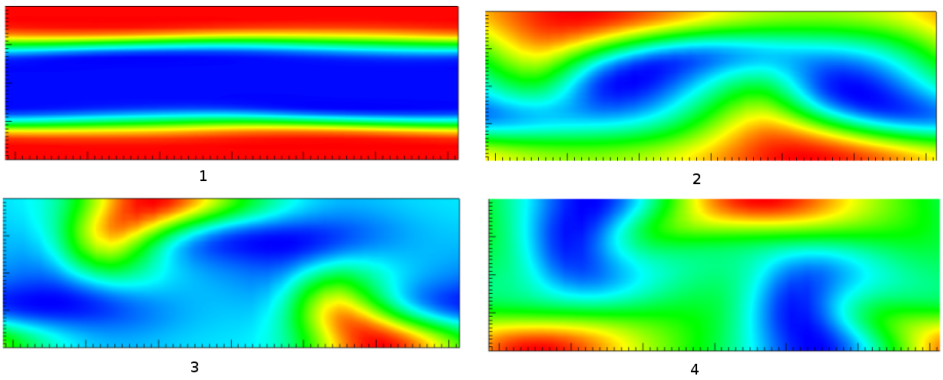

Figure 6.10: Snapshot at different time of mixing with second type of initial condition. Kz=0, kx=1, ky=pi.

enhance the mixing also in the transient cases. Hence we believe that the optimal configurations found for the steady-state are the most convenient for practical purposes because can work properly even in transient regimes.

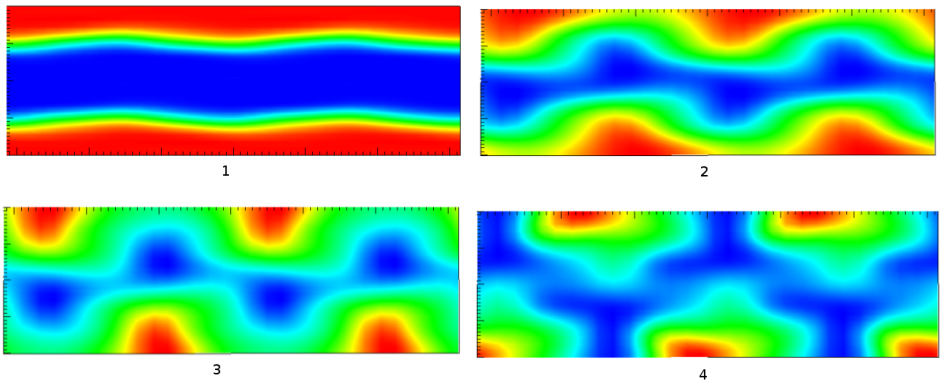

Figure 6.11: Snapshot at different time of mixing with first type of initial condition. Kz=0, kx=2, ky=2pi.

Chapter 7

Conclusions

7.1 Conclusions

This master thesis project focused on the study of mass transfer in a fluid flowing through a variable porosity medium inside a channel. This is a crucial problem in several applications such as Fuel Cells and Flow Batteries. The final aim of the project was to assess the possibility to increase the mixing and the mass transfer varying the local porosity inside the medium.

The study has been performed using Direct Numerical Simulations of the Volume-Average-Navier-Stokes (VANS) equations with scalar transport. To this purpose the open-source parallel code NEK5000 developed at Argonne National Laboratories has been expanded implementing the additional terms present in the VANS equations.

Two different classes of problems have been studied: the former pertaining to steady-state conditions, the latter to transient dynamics. The medium examined has a bulk porosity of 0.7. Several simulations modulating the local porosity of the medium via harmonic functions have been performed to evaluate how the mass transfer can be enhanced respect the reference case with uniform porosity.

Focusing on the steady-state cases, the mass transfer between the two walls with imposed scalar values of a laminar channel is evaluated together with other dynamical quantities, e.g. velocity fields, streamlines... The modulation of the porosity induces secondary motions that are able to excite the convective transport enhancing the overall mass transport and mixing. Optimal configurations are able to increase the overall mixing up to 40%. In general configurations where the porosity is varied with wider wavelengths perform better. Actually, optimal mass transfer is obtained using the longest porosity modulation between the walls, i.e. only one wave. Different is the dynamics imposed by the porosity modulation in the streamwise direction where there is not an upper bound for the wave length. Actually, the longest wave length coincides with cases where the porosity changes only in the wall normal direction and convective motions are not excited. Hence it exists an optimal frequency of modulation in the streamwise direction that has been extracted in some configurations where the the porosity geometry is not changed in the other directions. A dimensional model based on the comparison of the typical diffusive and convective time scales of the phenomena is proposed to determine the ideal streamwise modulation (given the wall-normal modulations). Optimal configurations occur when the two time scales assume the same order of magnitude, see sec 4.3.2. The model, though a little bit rough, performs reasonably well for 2D cases. On this aspect, it should be noted that, using harmonic functions to modulate the porosity in the medium, the highest mass transfer enhancement has been obtained in 2D cases where there is no modulation in the spanwise direction.

The analysis of the transient-state dynamics has been performed imposing null scalar flux at the walls and evolving an initial conditions where the scalar concentration field was constituted by slots with uniform value. Then the time needed for homogenization has been evaluated looking at the scalar variance evolutions. Even for these cases the porosity modulation was able to enhance the overall mix-

ing exciting the convective transport via secondary motions. These cases are less sensitive to the details of the porosity modulations and all the optimal configurations found in the steady-state cases perform well. Actually, depending on the initial conditions, in the present cases also other porosity modulations with higher frequency may enhance the mixing. The important point is that the secondary motions should occur near the concentration gradient.

Hence, we conclude that modulating the porosity of a medium it is possible to enhance the mass transfer. For a guideline to design optimal configurations we suggest to use the longest wavelength in the wall normal direction, i.e. one period only. We also advice to use a 2D geometry without modulations of the porosity in the spanwise directions. Concerning instead the modulation in the streamwise direction, the optimal frequency can be estimated imposing a match of the typical diffusive and convective time scales, see section 4.3.2. From a practical perspective, a convening solution could be to use a porous medium constituted by blocks of different porosity which should be thick as the half width of the channel and with an odd placement in the wall-normal and streamwise directions. This could mimic the optimal sinusoidal modulation found in this work, but with a clear production simplicity, see fig. 7.1.

7.2 Future developments

For a full comprehension of the present results further investigations are needed. Starting from the actual dataset, it would be interesting to simulate porosity modulation with more frequency values of the porosity function in order to determine more trends to support the present findings.

On the other side, it is certainly interesting to experimentally prove the present findings in order to see how effective is the real enhancement in the mass transfer.

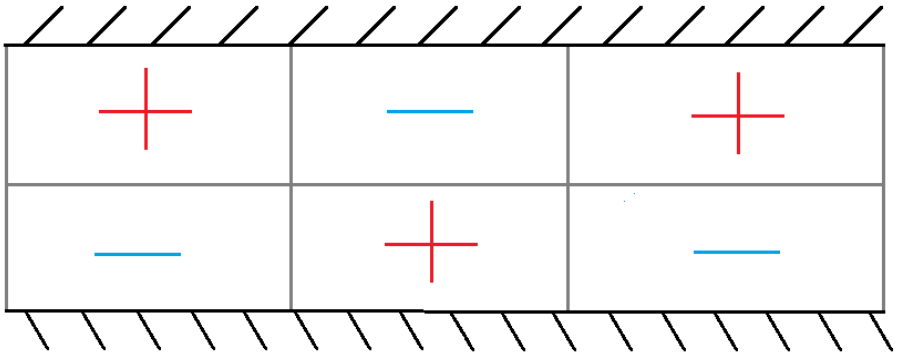

Figure 7.1: Sketch of the transport process occurring in the porous media when more oscillations in the wall normal direction are considered.

This part is crucial in order to proceed towards a technological advancement of all the devices where is important a fast mixing of the flow in a porous medium, e.g. Redox-Flow Battery.

Acknowledgments

Il ringraziamento più grande è per i miei genitori. Il vostro impegno e la fatica quotidiana mi sono stati da stimolo per dare il massimo in ogni cosa in questi anni. Non c'è modo per ringraziarvi per tutti i sacrifici che avete fatto per rendere felici me e mia sorella. Per me, sarete per sempre il miglior esempio da seguire.

Grazie a Serena! Dovrei ringraziarti per un'infinità di cose per questi 5 anni..grazie per esserci sempre stata, per rendermi felice e per essere la persona meravigliosa che sei.

Grazie a Martina perchè, anche se forse non sembra, ci vogliamo davvero bene. So di poter contare sempre su di te e per me, sei la migliore sorella di tutte.

Grazie a tutti i miei amici del BT. Anche se i nostri futuri non saranno nella mitica Battaglia Terme, i veri amici come voi resteranno per sempre, insieme a tutti i ricordi trascorsi insieme.

Grazie a Luca e Francesco per la magnifica opportunità che mi avete concesso. Grazie per tutti gli insegnamenti e l'aiuto che mi avete dato, ho imparato molto con voi. Grazie soprattutto perchè in questi mesi, oltre che davvero bravi professori, siete stati come degli amici.

Grazie infine a tutte le persone che mi sono state vicine. La presenza di ognuno di voi mi ha permesso di raggiungere questo obiettivo!

Thank God, ce l'ho fatta!

Bibliography

[Bear(1972)] Bear, J. 1972 *Dynamics of Fluids in Porous Media*. Dover.

[Bugga *et al.*(2013)Bugga, West, Kindler & Smart] Bugga, R. V., West, W. C., Kindler, A. & Smart, M. C. 2013 New class of flow batteries for terrestrial and aerospace energy storage applications .

[Howes & Whitaker(1985)] Howes, F. A. & Whitaker, S. 1985 The spatial averaging theorem revisited. *Chemical Engineering Science* **40** (8), 1387 – 1392.

[Hussong *et al.*(2011)Hussong, Breugem & Westerweel] Hussong, J., Breugem, W.-P. & Westerweel, J. 2011 A continuum model for flow induced by metachronal coordination between beating cilia. *Journal of Fluid Mechanics* **684**, 137–162.

[Jhon D. Anderson(2001)] Jhon D. Anderson, J. 2001 *Foundamentals of Aerodynamics (3rd. edition)*. McGraw-Hill Education.

[Kee & Gavriilidis(2008)] Kee, S. P. & Gavriilidis, A. 2008 Design and characterisation of the staggered herringbone mixer. *Chemical Engineering Journal* **142** (1), 109 – 121.

[Kundu P.K.(2004)] Kundu P.K., C. I. 2004 *Fluid Mechanics (3rd. edition)*. Elsevier.

[Malm(2011)] Malm, J. 2011 Spectral-element simulations of turbulent wall-bounded flows including transition and separation. PhD thesis, KTH, Stability, Transition and Control, qC 20111206.

[Paul F. Fischer & Kerkemeier(2008)] Paul F. Fischer, J. W. L. & Kerkemeier, S. G. 2008 nek5000 Web page. Http://nek5000.mcs.anl.gov.

[Pope(2000)] Pope, S. B. 2000 *Turbulent Flows.*. Cambridge University Press.

[Shah *et al.*(2008)Shah, Watt-Smith & Walsh] Shah, A., Watt-Smith, M. & Walsh, F. 2008 A dynamic performance model for redox-flow batteries involving soluble species. *Electrochimica Acta* **53** (27), 8087 – 8100.

[Whitaker(1996)] Whitaker, S. 1996 The forchheimer equation: a theoretical development. *Transport in Porous media* **25** (1), 27–61.

[Whitaker(1999)] Whitaker, S. 1999 *The method of volume averaging*, , vol. 13. Springer Science & Business Media.

[You *et al.*(2009)You, Zhang & Chen] You, D., Zhang, H. & Chen, J. 2009 A simple model for the vanadium redox battery. *Electrochimica Acta* **54** (27), 6827 – 6836.